UNIVERSIDADE FEDERAL DE JUIZ DE FORA
INSTITUTO DE CIÊNCIAS EXATAS
PÓS-GRADUAÇÃO EM CIÊNCIA DA COMPUTAÇÃO

Hemerson Aparecido da Costa Tacon

Data Augmentation of Visual Rhythms using Symmetric Extension for Deep Learning Video Based Human Action Recognition

Juiz de Fora

2019

UNIVERSIDADE FEDERAL DE JUIZ DE FORA
INSTITUTO DE CIÊNCIAS EXATAS
PÓS-GRADUAÇÃO EM CIÊNCIA DA COMPUTAÇÃO

Hemerson Aparecido da Costa Tacon

Data Augmentation of Visual Rhythms using Symmetric Extension for Deep Learning Video Based Human Action Recognition

Dissertação apresentada ao Programa de Pós-Graduação em Ciência da Computação, do Instituto de Ciências Exatas da Universidade Federal de Juiz de Fora como requisito parcial para obtenção do título de Mestre em Ciência da Computação.

Orientador: Marcelo Bernardes Vieira

Juiz de Fora

2019

Hemerson Aparecido da Costa Tacon

Data Augmentation of Visual Rhythms using Symmetric Extension for Deep Learning Video Based Human Action Recognition

Dissertação apresentada ao Programa de Pós-Graduação em Ciência da Computação, do Instituto de Ciências Exatas da Universidade Federal de Juiz de Fora como requisito parcial para obtenção do título de Mestre em Ciência da Computação.

Aprovada em 11 de Junho de 2019.

BANCA EXAMINADORA

Prof. D.Sc. Marcelo Bernardes Vieira - Orientador
Universidade Federal de Juiz de Fora

Prof. D.Sc. Saulo Moraes Villela
Universidade Federal de Juiz de Fora

Prof. D.Sc. Hélio Pedrini
Universidade Estadual de Campinas

Ficha catalográfica elaborada através do programa de geração
automática da Biblioteca Universitária da UFJF,
com os dados fornecidos pelo(a) autor(a)

Tacon, Hemerson Aparecido da Costa.
Data augmentation of visual rhythms using symmetric extension for deep learning video based human action recognition / Hemerson Aparecido da Costa Tacon. -- 2019.
88 f. : il.

Orientador: Marcelo Bernardes Vieira
Dissertação (mestrado acadêmico) - Universidade Federal de Juiz de Fora, ICE/Engenharia. Programa de Pós-Graduação em Ciência da Computação, 2019.

1. Deep Learning. 2. Human Action Recognition. 3. Data Augmentation. 4. Visual Rhythm. 5. Video analysis. I. Vieira, Marcelo Bernardes, orient. II. Título.

AGRADECIMENTOS

Primeiramente, eu gostaria de agradecer à minha família que sempre incentivou meus estudos durante toda essa jornada, e por todo o esforço empenhado em minha educação e criação. Agradeço também pela compreensão nos momentos em que não pude estar com vocês em minha cidade natal, e também nos momentos em que eu estava lá mas não podia dar muita atenção, pois estava ocupado com afazares acadêmicos.

Sou grato também a todos os professores do DCC e do PGCC que, de alguma forma, contribuíram na minha formação, e também pelos ensinamentos passados durante todos esses anos de graduação e de mestrado. Em especial, agradeço ao professor Marcelo Bernardes pela ideia de tema de pesquisa e pela orientação. Agradeço também a todos os colegas e amigos da UFJF pelos vários momentos de conversa, risadas e troca de ideias durante essa jornada. Agradeço principalmente aos meus parceiros de GCG e de mestrado, André e Hugo, com quais compartilhei incertezas, frustrações, códigos, inúmeras caronas e também cada resultado positivo durante essa nossa empreitada de aprender Deep Learning praticamente sozinhos. Agradeço também à colaboração com o pessoal do LIV na Unicamp, e em especial à Helena pela imensurável ajuda executando meus scripts em algumas máquinas da Unicamp e também pela troca de ideias.

Agradeço aos funcionários da UFJF e do PGCC pelo suporte. Agradeço à CAPES pelo apoio financeiro sem o qual eu não teria conseguido realizar este mestrado. Agradeço também à NVIDIA pela doação de placas de vídeo sem as quais eu teria conseguido executar apenas uma pequena fração dos milhares (não estou exagerando) de experimentos que realizei.

Finalmente, agradeço à Dalila. Só você tem noção do real esforço que foi empenhado durante este mestrado e esteve do meu lado durante toda essa caminhada, não me deixando desanimar, sendo meu porto seguro. Muito obrigado!

"Artificial Intelligence is the new electricity." Andrew Ng.

RESUMO

Nos últimos anos, avanços significativos foram alcançados no problema de classificação de imagens devido ao aprimoramentos dos modelos de Aprendizagem Profunda. Entretanto, no que diz respeito ao Reconhecimento de Ações Humanas, ainda existe muito espaço para melhorias. Uma forma de melhorar o desempenho de tais modelos é através do aumento de dados. Dessa forma propomos, como aumento de dados, o uso de múltiplos recortes do Ritmo Visual, simetricamente estendidos no tempo e separados por uma distância fixa. Propomos ainda utilizar uma nova forma de extração do Ritmo Visual, o Ritmo Visual Ponderado. Este método propõe reforçar os padrões de movimento pesando os aspectos mais próximos de uma posição específica no vídeo na qual julgamos que a ação tenha maior probabilidade de ocorrer. O método final consiste na replicação do Ritmo Visual Ponderado concatenando quantas cópias forem necessárias ao longo da dimensão temporal, tendo as cópias pares invertidas horizontalmente. Esse método torna possível a extração de recortes que correspondam ao tamanho de entrada fixo da Rede Neural Convolucional utilizada, bem como a preservação da taxa de amostragem do vídeo, o que é crucial para não distorcer a velocidade das ações. Não obstante, os vários recortes garantem que toda extensão espacial e temporal do Ritmo Visual seja contemplada. Com o objetivo de avaliar nosso método, empregamos uma estratégia multi-fluxo. Essa estratégia consiste na combinação de informações extraídas a partir dos frames RGB dos vídeos, do Fluxo Ótico, e dos Ritmos Visuais Simetricamente Estendidos horizontal e vertical. Nosso método resultou em taxas de acurácia próximas ao estado da arte nos conjuntos de dados UCF101 e HMDB51.

Palavras-chave: Aprendizagem Profunda. Reconhecimento de Ações Humanas. Aumento de Dados. Ritmo Visual. Análise de Vídeos.

ABSTRACT

Despite the significant progress of Deep Learning models on the image classification task, they still need enhancement for efficient Human Action Recognition. Such gain could be achieved through the augmentation of the existing datasets. With this goal, we propose the usage of multiple Visual Rhythm crops, symmetrically extended in time and separated by a fixed stride. The premise to augment the temporal dimension of the Visual Rhythms is that the direction of video execution does not discriminate several actions. Besides that, we propose to use the Weighted Visual Rhythm: its extraction method attempts to reinforce motion patterns by weighing the closest aspects of a specific video position in which the action typically occurs. Therefore, we replicate the Weighted Visual Rhythm by concatenating, along the temporal dimension, as many as necessary copies of it, having the even copies horizontally flipped. While providing the possibility of extracting crops matching the fixed input size of the Convolutional Neural Network employed, the symmetric extension preserves the video frame rate, which is crucial to not distort actions. In addition, multiple crops with stride ensure the coverage of the entire video. Therefore, the main contributions of this work are a new form of extracting the Visual Rhythm and a new method for performing the data augmentation of video samples. Aiming to evaluate our method, a multi-stream strategy combining RGB and Optical Flow information is modified to include two additional spatiotemporal streams: one operating on the horizontal Symmetrically Extended Visual Rhythm, and another operating on the vertical Symmetrically Extended Visual Rhythm. Accuracy rates close to the state of the art were obtained from the experiments with our method on the challenging UCF101 and HMDB51 datasets.

Keywords: Deep Learning. Human Action Recognition. Data Augmentation. Visual Rhythm. Video analysis.

LIST OF FIGURES

2.1 Top1 *vs.* operations $\propto$ parameters. Top-1 one-crop accuracy versus the number of operations required for a single forward pass. The size of the blobs is proportional to the number of network parameters. The red rectangle highlights the employed network, InceptionV3. Adapted from "An Analysis of Deep Neural Network Models for Pratical Applications" (CANZIANI et al., 2016). 24

2.2 Inception module. For computational efficiency, the yellow blocks perform 1×1 convolutions with the purpose of dimensionality reduction, while the other blocks perform all considered operations instead of choosing one of them. Adapted from "Going Deeper with Convolutions" (SZEGEDY et al., 2015). 25

2.3 Enhanced inception modules with convolution factorization. The 5×5 kernel is replaced by two 3×3 convolutions in (a) and all 3×3 convolutions are replaced by sequences of $1 \times n$ and $n \times 1$ convolutions in (b). Adapted from "Rethinking the Inception Architecture for Computer Vision" (SZEGEDY et al., 2016). 26

2.4 Optical Flow of a sample of the *biking* class from UCF101 dataset decomposed into horizontal and vertical components. The vertical leg movement is captured by the vertical component, and, similarly, the background horizontal movement is captured by the horizontal component (yellow and red dashed rectangles, respectively). 29

2.5 Example of horizontal and vertical Visual Rhythms of a sample video of the class *biking* from UCF101 dataset. The horizontal and vertical rhythms were taken from the central row and column, respectively. 31

4.1 Final multi-stream architecture. The training of each stream is performed individually, and a weighted sum of the feature maps determines a descriptor utilized in the final classification. 46

4.2 Weighted Visual Rhythm of a sample video of the class *biking* from UCF101 dataset: y is the middle row in the horizontal rhythm (a), and x is the middle column in the vertical rhythm (b), and σ_x and σ_y are both equal to 33. 48

4.3 Different Visual Rhythm versions of the same video sample of the class *biking* from UCF101 dataset. First row (a-d) consists of the horizontal versions and the second one (e-h) consists of the vertical versions. From left to right: simple Visual Rhythm, Weighted Visual Rhythm, and mean Visual Rhythm colored and in grayscale. The simple rhythms used the middle row and column as reference lines, and the weighted rhythms used $\alpha_x = \alpha_y = 0.5$ and $\sigma_x = \sigma_y = 33$. 49

4.4 Up-sampling of two different Visual Rhythms from HMDB51 dataset. The yellow rectangles highlight the main action pattern of each rhythm. Notice that, after the transformation, the angles of inclination of each action pattern become closer to each other in contrast to the obvious distinction between them previously. 51

4.5 Extraction of five squared crops from the symmetric extensions of both horizontal (a) and vertical (b) Visual Rhythms of the same video of the class *biking* from UCF101 dataset. The frame width is $w = 320$ pixels, the frame height is $h = 240$ pixels, and the corresponding video length is $f = 240$ frames. The stride between crops is $s = 150$ pixels and the crop dimensions are $w_{CNN} = h_{CNN} = 299$. The central area in X is selected in (a) and in (b) the rhythm will be stretched in Y to cover the crop dimensions. 52

4.6 Overview of the proposed Visual Rhythm stream. After the symmetric extension, n_c crops apart from each other by a stride s are extracted in the center (yellow). Depending on the dataset, extra crops aligned with the image top (magenta) and bottom (cyan) are extracted. All crops are applied to the CNN. The resulting features are averaged, and the final class is predicted through a softmax layer. 55

5.1 Mean accuracy difference for each class between SEVR_y and WVR_y for UCF101 (a) and HMDB51 (b). Blue bars indicate that SEVR performs better by the given amount while red bars favor WVR. 65

5.2 Mean accuracy difference for each class between SEVR_x and WVR_x for UCF101 (a) and HMDB51 (b). Blue bars indicate that SEVR performs better by the given amount while red bars favor WVR. 69
5.3 Mean confusion matrix of the final multi-stream method for UCF101. 75
5.4 Mean confusion matrix of the final multi-stream method for HMDB51. 76

LIST OF TABLES

5.1 Baseline accuracy rates (%) for UCF101 and HMDB51. 59

5.2 Comparison of accuracy rates (%) for UCF101 and HDMB51 varying the σ_y parameter. 61

5.3 Comparison of mean accuracy rates (%) of UCF101 and HMDB51 varying the α_y factor. 61

5.4 Comparison of accuracy rates (%) of UCF101 and HMDB51 datasets varying n_c parameter. 62

5.5 Percentage of samples that are extended according to the employed stride s, with $w_{CNN} = 299$ and $n_c = 4$. 63

5.6 Comparison of accuracy rates (%) for UCF101 and HMDB51 varying the stride s parameter. 63

5.7 Comparison of accuracy rates (%) for UCF101 and HMDB51 when extra crops are used. 64

5.8 Comparison of accuracy rates (%) for UCF101 and HDMB51 varying the σ_x parameter. 66

5.9 Comparison of mean accuracy rates (%) of UCF101 and HMDB51 varying the α_x factor. 67

5.10 Comparison of accuracy rates (%) of UCF101 and HMDB51 datasets varying n_c parameter. 67

5.11 Comparison of accuracy rates (%) for UCF101 and HMDB51 varying the stride s parameter. 68

5.12 Comparison of accuracy rates (%) for UCF101 and HMDB51 when extra crops are used. 68

5.13 Comparison of accuracy rates (%) for UCF101 and HMDB51 with (w/) and without (w/o) data augmentation methods. 70

5.14 Results of single-stream approaches. 71

5.15 Results of the combination of the streams. 73

5.16 Comparison of accuracy rates (%) for UCF101 and HMDB51 datasets. 74

LIST OF SYMBOLS

$d_i(u, v)$	dense flow field at the position (u, v) in frame i.
d_i^x	dense flow horizontal component.
d_i^y	dense flow vertical component.
$g(s, \sigma)$	Gaussian weighting function $g(s, \sigma) = e^{-\frac{s^2}{\sigma^2}}$.
p	point in frame $p = (u, v)$.
x	reference column.
y	reference row.
$C_{xt}(a, b)$	crop of a vertical visual rhythm with inferior left coordinates (a, b).
$C_{yt}(a, b)$	crop of a horizontal visual rhythm with inferior left coordinates (a, b).
F_i	frame i formed by the $h \times w$ matrix.
I_τ	optical flow stack at the frame τ.
P	set of 2D image coordinates $P = \{p_1, \cdots, p_n\}$.
S_i	1D contribution $S_i = [F_i(p_1)\ F_i(p_2)\ \cdots\ F_i(p_n)]^T$ of the i-th frame, with $F_i(p_j)$ representing the RGB value of the point p_j in the frame F_i.
$\mathrm{SEVR}_x(i, k)$	vertical symmetrically extended visual rhythm.
$\mathrm{SEVR}_y(i, k)$	horizontal symmetrically extended visual rhythm.
V	video $V = \{F_1, F_2, \cdots, F_f\}$.
VR_P	visual rhythm $\mathrm{VR}_P = [S_1\ S_2\ \cdots\ S_f]$ given a set of 2D image coordinates P.
WVR_y	horizontal weighted visual rhythm $\mathrm{WVR}_y = \sum_{r=1}^{h} \mathrm{VR}_{P_r} \cdot g(r - y, \sigma_y)$.
WVR_x	vertical weighted visual rhythm $\mathrm{WVR}_x = \sum_{c=1}^{w} \mathrm{VR}_{P_c} \cdot g(c - x, \sigma_x)$.
α_x	factor for the vertical visual rhythm positioning $x = \alpha_x \cdot w$.
α_y	factor for the horizontal visual rhythm positioning $y = \alpha_y \cdot h$.
σ_x	vertical standard deviation.
σ_y	horizontal standard deviation.

LIST OF ACRONYMS

AVR Adaptive Visual Rhythm

BoW Bag of Words

C3D Convolutional 3D

CNN Convolutional Neural Network

CV Computer Vision

DCNN Deep Convolutional Neural Network

DL Deep Learning

DNN Deep Neural Network

DTPP Deep networks with Temporal Pyramid Pooling

EEP Eigen Evolution Pooling

fps frames per second

GPU Graphics Processing Unit

GRU Gated Recurrent Unit

HAR Human Action Recognition

HoF Histogram of Optical Flows

HoG Histogram of Gradients

I3D Two-Stream Inflated 3D ConvNet

IDT Improved Dense Trajectories

MBH Motion Boundary Histograms

MDI Multiple Dynamic Images

MIFS Multi-skIp Feature Stacking

ML Machine Learning

NN Neural Network

OF Optical Flow

OFF Optical Flow guided Feature

PoE Product of Experts

PoTion Pose moTion

RANSAC RANdom SAmple Consensus

ReLU Rectified Linear Unit

ResNet Residual Network

RGB Red-Green-Blue

RNN Recurrent Neural Network

ROI Regions of Interest

SEVR Symmetrically Extended Visual Rhythm

SGD Stochastic Gradient Descent

SIFT Scale-Invariant Feature Transform

SOTA state of the art

ST-ResNet Spatiotemporal Residual Network

STCB Spatiotemporal Compact Bilinear

SURF Speeded-Up Robust Features

SVM Support Vector Machine

TDD Trajectory-pooled Deep-convolutional Descriptor

TLE Temporal Linear Encoding

TSM Temporal-Spatial Mapping

TSN Temporal Segment Networks

VR Visual Rhythm

WVR Weighted Visual Rhythm

CONTENTS

1 INTRODUCTION 18

1.1 PROBLEM DEFINITION 19

1.2 OBJECTIVES 19

1.3 CONTRIBUTIONS 20

1.4 METHODOLOGY 21

1.5 OUTLINE 22

2 FUNDAMENTALS 23

2.1 HUMAN ACTION RECOGNITION 23

2.2 NETWORK ARCHITECTURE 23

2.3 MULTI-STREAM ARCHITECTURE 25

2.4 RGB STREAM 27

2.5 OPTICAL FLOW STREAM 28

2.6 VISUAL RHYTHM 29

2.6.1 Visual Rhythm definition 31

3 RELATED WORK 33

3.1 HAND-CRAFTED FEATURE BASED APPROACHES 33

3.2 3D-BASED APPROACHES 35

3.3 MULTI-STREAM METHODS 36

3.3.1 Spatial feature based approaches 37

3.3.2 Temporal Feature based approaches 38

3.3.3 Spatiotemporal feature based approaches 41

3.3.4 Other approaches 42

3.4 DATA AUGMENTATION 43

4 PROPOSED METHOD 46

4.1 WEIGHTED VISUAL RHYTHM 47

4.2 SYMMETRIC EXTENSION 50

4.2.1 Symmetric Extension with Fixed Stride Crops 53

4.3 SPATIOTEMPORAL STREAM CLASSIFICATION PROTOCOL 54
4.4 MULTI-STREAM CLASSIFICATION PROTOCOL 56

5 EXPERIMENTAL RESULTS 57
5.1 DATASETS 57
5.2 IMPLEMENTATION DETAILS 58
5.3 HORIZONTAL VISUAL RHYTHM PARAMETERIZATION 60
5.4 VERTICAL VISUAL RHYTHM PARAMETERIZATION 66
5.5 DATA AUGMENTATION ABLATION STUDY 70
5.6 MULTI-STREAM CLASSIFICATION USING VISUAL RHYTHMS 71

6 CONCLUSIONS AND FUTURE WORK 77

REFERENCES 79

1 INTRODUCTION

In the last years, revolutionary advances were accomplished in the Computer Vision (CV) field. This progress is due to the development of Deep Learning (DL) methods, driven by the technological enhancements of Graphics Processing Unit (GPU) (GU et al., 2015). In this context, the major DL breakthrough was the Deep Convolutional Neural Network (DCNN) architecture for image classification known as AlexNet (KRIZHEVSKY et al., 2012). Since then, many other architectures for image classification were developed (SZEGEDY et al., 2015, 2016; HE et al., 2016). All these architectures benefited from the emergence of large image datasets, such as ImageNet (DENG et al., 2009). A natural consequence of this success was the exploitation of these achievements in the field of video classification. In this domain, one problem consists in recognizing the main action being represented by a person along a video. A solution to this problem is crucial to automate many tasks and it has outstanding applications: video retrieval, intelligent surveillance and autonomous driving (CIPTADI et al., 2014; JI et al., 2013; KONG; FU, 2018). This specific problem is called Human Action Recognition (HAR), and it is the subject of the present work.

In contrast to images, videos present the time dimension, which produces a considerable data increase. Although some approaches have used 3D Convolutional Neural Networks (CNNs) (JI et al., 2013; CARREIRA; ZISSERMAN, 2017), the additional temporal data generally makes this prohibitive. To avoid this, the majority of recent works predominantly use 2D CNNs for action recognition, and this choice requires a video volume representation in a 2D space (FEICHTENHOFER et al., 2017; CHOUTAS et al., 2018; WANG et al., 2018). The employed architectures generally have a fixed input size forcing the representations to match it. Another difference between the problems of image and video classification is the lack of massive labeled datasets for the latter. The existing ones (ABU-EL-HAIJA et al., 2016; KARPATHY et al., 2014) tend to have poorly annotations (KONG; FU, 2018). Thus, a workaround is to augment some well-established datasets (SOOMRO et al., 2012; KUEHNE et al., 2013). To this end, some manipulation of the time dimension may be demanded, since their video lengths vary between samples. However, such manipulation is not simple, and special cautions are required when per-

forming the augmentation. For instance, keeping the original video frame rate is critical for the action recognition problem. Any variation in the frame rate could alter the action speed and distort it. When attempting to classify a video with *walking* action, for example, this could be easily confused with the action of *running* if a video with the first action had its frame rate increased compared to a video containing the second action.

1.1 PROBLEM DEFINITION

The problem of Human Action Recognition in videos consist of identifying the main action being performed by an actor along a video. This problem is the focus of the present work. The actions are normally simple lasting for only a few seconds. However, the recognition process is dynamic since there is a diversity of nuances contrasting the actions. For instance, while some actions are constituted of only the motion of body parts, other actions have interactions with objects or other people. Therefore, the challenges of HAR relies on performing the defined process under different viewpoints, light conditions, pose orientations and in spite of significant differences in manner and speed that a video can present. In the present work, the visual aspects are the only considered information to classify the video. It is worth mentioning that other approaches could considerate other sensory channels such as video audio (BIAN et al., 2017), for instance.

The datasets employed in the present work define a specific set of actions. Each sample belong to one class of the pre-defined set. The datasets also present three distinct training and testing splits of the samples. Thus, the HAR problem can be classified as a supervised classification problem. The challenge in this context is to create a model capable of learning relevant aspects from the training set to recognize the actions of the samples in the testing set.

1.2 OBJECTIVES

Addressing the issues imposed by time dimension handling, this present work presents a method for HAR taking advantage of a DL architecture for classification. To achieve this objective, we propose the usage of Visual Rhythms (VRs) (NGO et al., 1999a,b; SOUZA, 2018; CONCHA et al., 2018). The VR is a 2D video representation with combined 1D Red-Green-Blue (RGB) information varying over time. The specific feature used in this

work to classify the videos is a variation of the VR proposed by Ngo et al. (1999a,b) and it is called Weighted Visual Rhythm (WVR).

As an extension of the primary objective, we present a data augmentation method for videos. This data augmentation is based on the Symmetrically Extended Visual Rhythm (SEVR). The symmetric extension in time assumes that most actions presented from back to front in time can be appropriately classified. That is, the direction of video execution does not discriminate several actions aspects. This method also allows the extraction of multiple VR crops without deformations in frame rate. In addition, the crop dimensions can also be set to match any required input size of the employed Neural Network (NN). All of these characteristics together make the symmetric extension a proper method to augment video datasets. As a secondary objective, we combine the proposed method with other notable methods of literature. When combined with other features in a multi-stream architecture, the VR provides complementary information, which is essential to reach accuracy rates close to state-of-the-art methods. We adapted the multi-stream architecture presented by Concha et al. (2018) to take RGB images, Optical Flow (OF) images and the SEVR images as inputs. In addition, we show that SEVR can improve the final classification accuracy.

Experiments were performed on two well-known challenging datasets, HMDB51 (KUEHNE et al., 2013) and UCF101 (SOOMRO et al., 2012), to evaluate our method. We slightly modified the widely known InceptionV3 network (SZEGEDY et al., 2016) to perform the experiments.

1.3 CONTRIBUTIONS

The contributions of this work are the following:

- WVR as a feature for video classification;
- Data augmentation for video datasets through the SEVR;
- The assessment of employ conventional data augmentation for image classification in the context of HAR with VRs;
- An extensive number of experiments attempting to find the best set of parameters for the proposed method.

1.4 METHODOLOGY

The literature research performed for this work revealed that multi-stream methods are currently the most successful approaches to deal with HAR. The majority of state-of-the-art works uses multi-stream to achieve the best results for video classification (CHOUTAS et al., 2018; CARREIRA; ZISSERMAN, 2017; WANG et al., 2016a). Taking advantage of the current state-of-the-art works, we put our efforts in the aggregation of a new type of feature that could complement the existing ones (RGB and OF) and thus achieve better results. To this end, the Visual Rhythm (VR) was chosen. This choice grounds on the VR's spatiotemporal nature, which contrasts to the RGB and OF feature types (spatial and temporal, respectively). There is evidence in the literature (DIBA et al., 2017; WANG et al., 2017a) supporting that spatiotemporal features are capable of capturing aspects that are not possible even after a late fusion of spatial and temporal features. Thus, we expect that the VR can be complementary to the other streams. Also, since VRs are represented by images, it is possible to take advantage of successful CNN architectures from the image classification problem.

The proposed VR approaches are based on two main hypotheses. The first one is that the main action in a video tends to occur in a more concentrated area of the video. We observed that usually, scenes are filmed aiming to frame the main event in the center of the video. Thus, a VR extraction considering this premise might represent better the underlying motion aspects of a video. Therefore, we propose to weight each line of information in the frames inversely proportional to the distance of them to a certain position, thus conceiving the WVR. Although the WVR presented superior results if compared to the mean VR (CONCHA et al., 2018), we have tried one more approach to increase its accuracy. Even though high accuracy is not a cause for a stream to be complementary when combined with others, a high accuracy certainly increases the likelihood that it complements the other streams. To this end, we explored data augmentation alternatives. Once more, we delved into the actions portrayed in the datasets and noticed that many of them could be reversed in time without any loss of characteristics. Thus, our second hypothesis is that many videos can have their execution direction reversed without harming the portrayed action. That is, the direction of execution of the video does not discriminate several actions, e.g., *brushing teeth*, *typing*, *clap*, *wave*, *pull ups*, etc. This allows us to use the videos executed in backward. In this way, we can extend the temporal dimension

of the rhythm by concatenating several copies of it having the even copies horizontally flipped and thus extract several crops from the same to be used as data augmentation.

To find out the best set of parameters for the SEVR, we chose to perform experiments varying the parameters incrementally. We have in mind that this approach does not ensure the optimal combination within the explored parameter space. However, we adopted this approach because of the high computational cost involved in the training of NNs together with the curse of dimensionality associated with the combinatorial space of the explored parameters. In addition, we verified the contribution of the data augmentation provided by our method separately of the conventional data augmentation methods used for image classification. The purpose was to assess the relevance of our approach to increase accuracy without any interference of other data augmentation methods and to determine the influence of common data augmentation methods for image classification in the context of VRs. Moreover, we verified all combinations of streams to evaluate the complementarity of each one of them with the others. Thus, we can confirm that all streams contribute to the accuracy of the final multi-stream architecture proposed in this work.

1.5 OUTLINE

The remainder of this work is organized as follows. The main concepts behind this work is the subject of Chapter 2. Chapter 3 presents a brief discussion about the works in literature. Chapter 4 presents the proposed methods of this work. These methods are evaluated in Chapter 5. The conclusion and futures works are the topics of Chapter 6.

2 FUNDAMENTALS

This chapter provides the main concepts about the employed network architecture, a brief discussion regarding multi-stream methods, and the fundamentals concerning the features used in the spatial, temporal, and spatiotemporal streams.

2.1 HUMAN ACTION RECOGNITION

In the context of Human Action Recognition (HAR), it is necessary to determine the meaning of some terms:

- **Action:** although there are many different definitions in the literature (TURAGA et al., 2008; CHAARAOUI et al., 2012; WANG et al., 2016b), we adopt the definition of action from Weinland et al. (2011). In the present work, the authors describe action as the whole process of a person performing a sequence of movements to complete a task. The person in this task can be interacting with other people or objects, such as a musical instrument;
- **Video descriptor:** it is a numerical representation of the video. The video descriptor is computed from the detected relevant aspects of the action performed. It has the form of a multi-dimensional vector;
- **Label:** the label is a denomination, such that a human agent can understand and perform the action described by it. For the HAR context, this denomination is usually a single verb or noun, or a verb together with a noun.

Therefore, the process of HAR in the videos can be split into the following steps: identify the relevant aspects of the movement and, with them, build a descriptor able to distinguish this set of features from others to obtain a class label for the video.

2.2 NETWORK ARCHITECTURE

In contrast to the network architectures used by Simonyan and Zisserman (2014a) (CNN-M-2048) and Wang et al. (2015b) (VGG-16 and GoogLeNet), in the present work, we

employed the InceptionV3 network (SZEGEDY et al., 2016). This network was chosen because of its superior performance for image classification in comparison with the previously used architectures. Moreover, if compared with other networks with better accuracy, the InceptionV3 has the advantage of performing fewer operations and using fewer parameters. Figure 2.1 illustrates such comparisons.

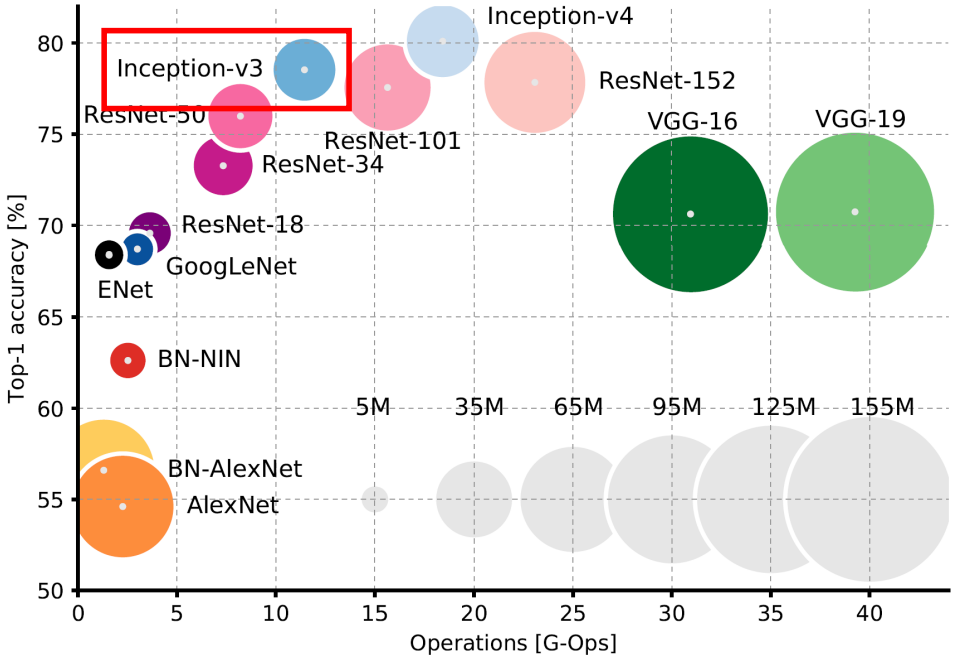

Figure 2.1: Top1 *vs.* operations $\propto$ parameters. Top-1 one-crop accuracy versus the number of operations required for a single forward pass. The size of the blobs is proportional to the number of network parameters. The red rectangle highlights the employed network, InceptionV3. Adapted from "An Analysis of Deep Neural Network Models for Pratical Applications" (CANZIANI et al., 2016).

The first version of the Inception network was presented by Szegedy et al. (2015). In that paper, the network was named GoogLeNet. Its main contribution was the creation of the inception modules. Instead of deciding which kernel size to use for a convolutional layer, they let the network perform them all. To this end, 1×1 convolutions are employed to reduce channel dimension of the feature maps and consequently reduce the cost involved into computing various convolutions in only one layer. The inception module also performs a pooling operation in one of its branches. These are the key ideas behind the inception module. Figure 2.2 depicts an inception module.

The second and third version of the Inception network were presented later with some enhancements (SZEGEDY et al., 2016). The authors reduced, even more, the computational cost of the convolutions in the inception modules. This was accomplished by

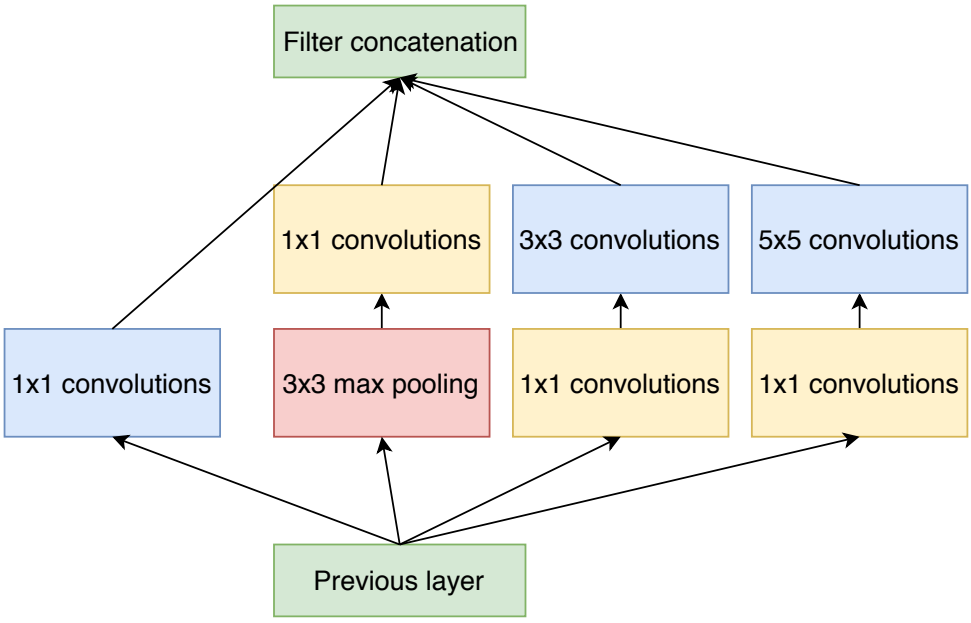

Figure 2.2: Inception module. For computational efficiency, the yellow blocks perform 1×1 convolutions with the purpose of dimensionality reduction, while the other blocks perform all considered operations instead of choosing one of them. Adapted from "Going Deeper with Convolutions" (SZEGEDY et al., 2015).

factorizing 5×5 convolutions with two 3×3 convolutions. They also proposed to factorize $n \times n$ convolutions with sequences of $1 \times n$ and $n \times 1$ convolutions. These factorizations are shown in Figure 2.3. The excellent performance of the InceptionV3, both in terms of speed and accuracy, was the determining factor for the choice of the same for the present work.

2.3 MULTI-STREAM ARCHITECTURE

Videos can be comprehended through their temporal and spatial aspects. The spatial part carries information about the appearance of the frame, such as background colors and shapes depicted in the video. The temporal part conveys the movement between the frames. Developing an architecture to work efficiently on these two aspects is an essential challenge in the area of HAR. DCNNs can be a supportive architecture in this subject, having the ability to extract high-level information from data observation instead of the hand-crafted descriptors designed by human experts (NANNI et al., 2017).

The precursory two-stream architecture presented by Simonyan and Zisserman (2014a) became the basis architecture to many subsequent works. Each stream of this architecture is basically a 2D CNN. The streams are trained separately. One of the streams operates

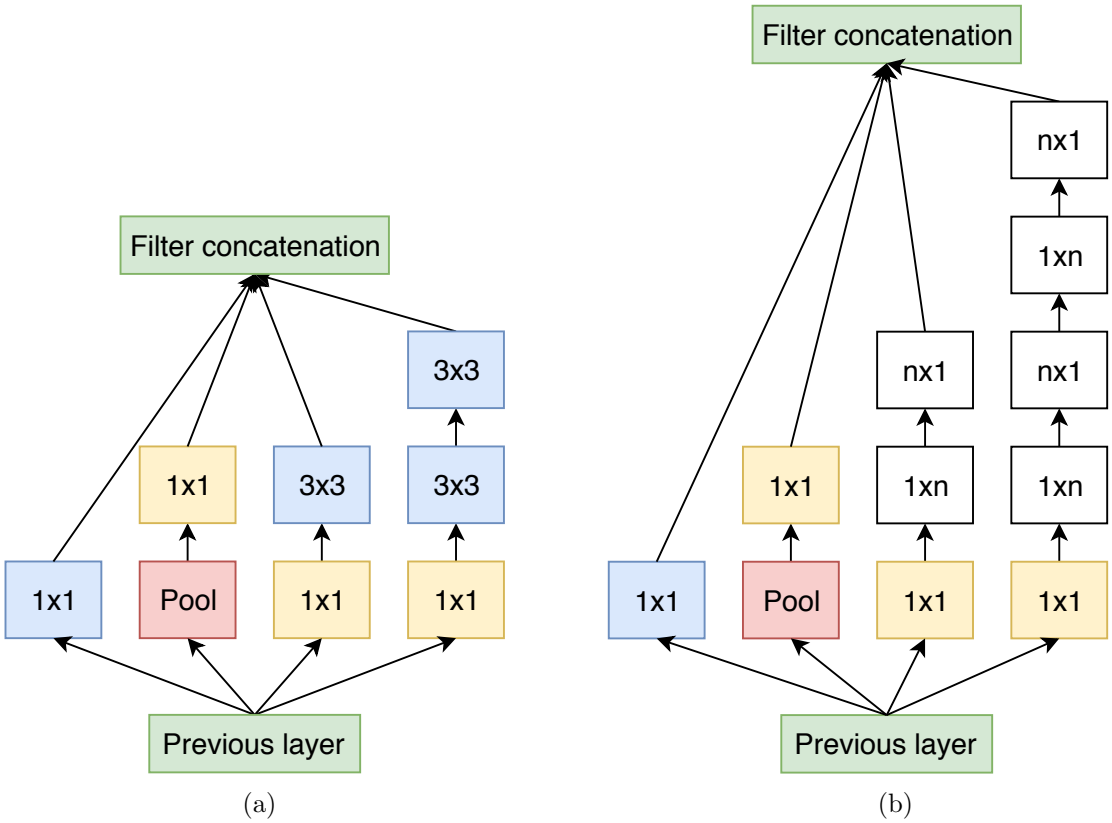

Figure 2.3: Enhanced inception modules with convolution factorization. The 5×5 kernel is replaced by two 3×3 convolutions in (a) and all 3×3 convolutions are replaced by sequences of $1 \times n$ and $n \times 1$ convolutions in (b). Adapted from "Rethinking the Inception Architecture for Computer Vision" (SZEGEDY et al., 2016).

on still RGB frames, and it is trained to learn spatial features. The other stream is fed with stacks of OF fields from multiple frames, and it is trained to learn temporal features. The final prediction is obtained by combining the softmax scores of both streams in a late-fusion manner. This basis two-stream architecture was later improved in the work of Wang et al. (2015b). In the present work, we follow these improvements together with the modification proposed by Concha et al. (2018) for the spatial stream.

Furthermore, we add other two streams creating a multi-stream architecture with four streams: the temporal stream presented by Wang et al. (2015b), the improved spatial stream proposed by Concha et al. (2018), and two spatiotemporal streams. The additional streams take as input two distinct VRs and have the goal of learning spatiotemporal features complementary to the other streams. The two classical streams are described and discussed in the following subsections.

2.4 RGB STREAM

A frame in a video corresponds to only a fraction of second. Although some human actions are performed very quickly, it is virtually impossible for an action to take only a fraction of a second to complete. However, in some cases, it is possible to reduce drastically the space of possible actions being performed in a video with the information of only one frame. Some actions are strongly associated with particular objects (SIMONYAN; ZISSERMAN, 2014a). This is the case of playing some musical instrument or practicing some sport with a ball. In the first case, there is a high chance that with only one frame, the musical instrument can be determined and the action portrayed in the video can be recognized. However, in the second case, perhaps more than one frame is needed to distinguish which sport is being practiced.

This strong association between action and object is a factor that makes the action recognition in video reach competitive results using only the information provided by a static image (SIMONYAN; ZISSERMAN, 2014a). Another determining factor for this was the significant advances in image classification achieved in recent years. Simonyan and Zisserman (2014a) used a CNN pre-trained on the ImageNet dataset (DENG et al., 2009) for the RGB stream and achieved fairly competitive results. These results culminated on the usage of the RGB stream in several posterior multi-stream approaches for HAR.

As mentioned before, sometimes one frame can be not enough to distinguish, for instance, the practice of two different sports with a ball. Also, significant changes during the time would not be perceived with only one frame. Trying to circumvent this problem, in the present work, we adopt the improved spatial stream proposed by Concha et al. (2018). It consists of training the spatial stream network with two frames per video sample: one frame randomly selected from the first half and another frame randomly chosen from the second half. The spatial stream receives each of both frames at a time. Even with this approach, some actions are heavily dependent on temporal features to be discerned, e.g., *walk* and *run*. These aspects made the temporal stream have a critical role in multi-stream approaches.

2.5 OPTICAL FLOW STREAM

The OF is a method for estimating and quantifying a pixel motion between subsequent frames (ZACH et al., 2007). Essentially, the OF is a 2D displacement vector of the apparent velocities of brightness patterns in an image (HORN; SCHUNCK, 1981). It has several applications in computer vision area, such as object detection (ASLANI; MAHDAVI-NASAB, 2013), video stabilization (LIU et al., 2014), and image segmentation (SEVILLA-LARA et al., 2016).

The OF is obtained by computing a dense flow field where each vector $d_i(u, v)$ represents the movement of a point $p = (u, v)$ between two consecutive frames, respectively, i and $i+1$. The OF vector field can be decomposed into horizontal and vertical components, d_i^x and d_i^y, and interpreted as channels of an image. In this way, it is possible to employ an efficient CNN to operate on OF images and perform action recognition. Simonyan and Zisserman (2014a) proposed to stack the flow channels $d_i^{x,y}$ of L consecutive frames, resulting in an input image with $2L$ channels. More formally, let $V = \{F_1, F_2, \cdots, F_f\}$ be a video with f frames F_i, where each frame is a $h \times w$ matrix. Thus, the input volume of an arbitrary frame τ given by $I_\tau \in R^{h \times w \times 2L}$ is defined as:

$$\begin{aligned} I_\tau(u, v, 2l-1) &= d^x_{\tau+l-1}(u, v) \\ I_\tau(u, v, 2l) &= d^y_{\tau+l-1}(u, v), \qquad l = \{1, \ldots, L\}. \end{aligned} \tag{2.1}$$

For any point $p = (u, v)$, with $u = \{1, \ldots, h\}$ and $v = \{1, \ldots, w\}$, the element $I_\tau(u, v, z)$, where $z = \{1, \ldots, 2L\}$, encodes the motion of p over a sequence of frames L defined in the video volume V. Figure 2.4 illustrates the OF computation and decomposition. Although the movements between one frame and another are small, the OF manages to capture these changes. Observe in Figure 2.4, inside the yellow dashed rectangle, the pattern formed in the vertical component by the leg movement. Similarly, inside the red dashed rectangle, the horizontal movement of the background create some patterns in the horizontal component.

In the scope of video classification, Simonyan and Zisserman (2014a) introduced the usage of OF sequences as temporal features in order to complement RGB-based CNNs used in this domain. The authors argued that the explicit motion description provided

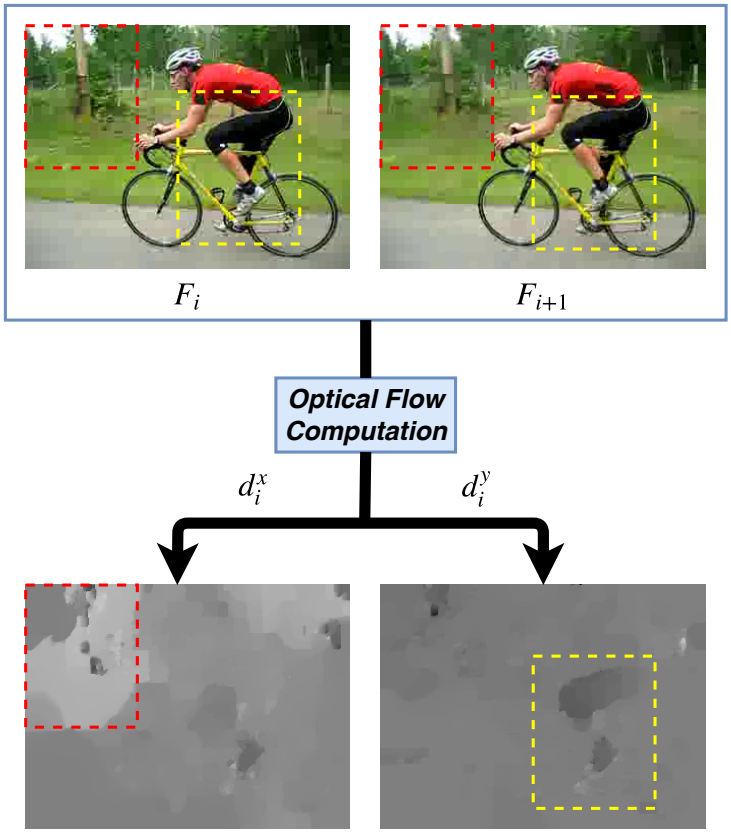

Figure 2.4: Optical Flow of a sample of the *biking* class from UCF101 dataset decomposed into horizontal and vertical components. The vertical leg movement is captured by the vertical component, and, similarly, the background horizontal movement is captured by the horizontal component (yellow and red dashed rectangles, respectively).

by the OF makes the recognition easier because the network does not need to determine motion implicitly. This approach achieved, even on small datasets, satisfactory accuracy rates (SIMONYAN; ZISSERMAN, 2014a). For these reasons, in the present work, the OF is adopted as the temporal stream to complement the RGB stream. We also utilize two extra spatiotemporal streams based on the VRs to complement even more recognition in time.

2.6 VISUAL RHYTHM

The VR is a spatiotemporal feature, in which a spatial dimension (X or Y axis) and the temporal dimension are aggregated into a 2D feature. It can be interpreted as a spatiotemporal slice of a video, i.e., a predefined set of pixels forming an arbitrary 2D surface embedded in a 3D volume of a video. By extracting the VR from videos, we attempt to reduce the HAR problem to image classification, which is advantageous because

of the already mentioned successful CNNs for this problem.

The term VR was first mentioned in the context of video icons to define the top and side view of a video icon (ZHANG; SMOLIAR, 1994). Despite being employed for the first time to detect camera transitions (cut, wipe and dissolve) (NGO et al., 1999a,b), the generalized idea of the VR that we use in this work was only later defined by Kim et al. (2001). This last work used VR to additionally detect zoom-in and zoom-out camera transitions.

Another task that can be performed using VRs is the automatic detection of captions (VALIO et al., 2011). A VR that contemplates a caption area presents notable rectangle patterns, which are not hard to detect. Pinto et al. (2012) proposed the usage of a VR analysis to deal with the problem of video-based face spoofing. The study was based on noise signatures detection in the VR representation obtained from the recaptured video Fourier spectrum.

The first employment of VRs in the HAR problem was accomplished by Torres and Pedrini (2016). They utilized high-pass filters to obtain Regions of Interest (ROI) in the VRs. It was argued that the action patterns were presented in only some parts of the VR. However, their approach for action recognition problem was evaluated on two datasets (KTH and Weizmann) which are considered small nowadays.

In a previous work, Concha et al. (2018) introduced the usage of VR combined with multi-stream models. The VR was employed as a spatiotemporal feature allowing interactions between time and space. These interactions improved the results of a well-known architecture. Another contribution of that work was a method to detect a better direction (horizontal or vertical) to extract the VR. The criterion was to use the VR of the direction with predominant movement.

In the present work, we show that the usage of a proper data augmentation technique for VRs can increase even more the accuracy obtained solely by it and, furthermore, improve the final accuracy of a multi-stream method. We also show that, in contrast to the gray-scale VR used in the work of Concha et al. (2018), the employment of colored VRs are essential to give important clues about the class represented by a sample. For instance, classes such as *breast stroke* and *diving* are always associated with a poll, which leaves remarkable blue patterns in the generated VR.

2.6.1 Visual Rhythm definition

Among the literature works, there are some variations in the VR definition. In this work, we adopted, with minor changes, the definition presented by Concha et al. (2018). Let $V = \{F_1, F_2, \cdots, F_f\}$ be a video with f frames F_i, where each frame is a $h \times w$ matrix, and $P = \{p_1, \cdots, p_n\}$ a set of 2D image coordinates. The 1D contribution of the i-th frame is given by the $n \times 1$ column vector $S_i = [F_i(p_1)\ F_i(p_2)\ \cdots\ F_i(p_n)]^T$, with $F_i(p_j)$ representing the RGB value of the point p_j in the frame F_i. Then, the VR for the entire video V is given by the $n \times f$ matrix:

$$VR_P = [S_1\ S_2\ \cdots\ S_f] \tag{2.2}$$

In most cases, the trajectory that is formed by the points in P is compact, and thus the VR represents a 2D subspace embedded in video volume XYT. For instance, if P is the set of points of a single frame row, the resulting VR is a plane parallel to XT. Analogously, setting P as a single frame column results in a plane that is parallel to YT. We call these VRs horizontal and vertical, respectively. Figure 2.5 exemplifies both horizontal and vertical VRs of a sample video of the class *biking* from the UCF101 dataset. In this example, the VR computation uses the central planes in both directions.

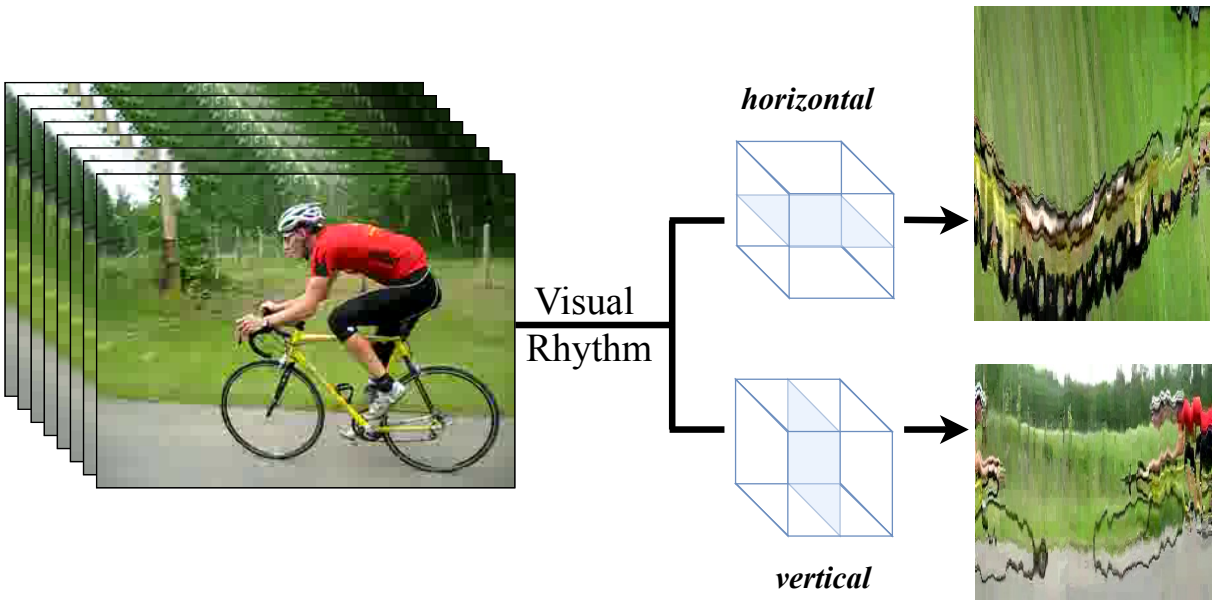

Figure 2.5: Example of horizontal and vertical Visual Rhythms of a sample video of the class *biking* from UCF101 dataset. The horizontal and vertical rhythms were taken from the central row and column, respectively.

Despite the other plans mentioned in the literature to extract the VR (e.g., diagonal (KIM et al., 2001), zig-zag (VALIO et al., 2011; TORRES; PEDRINI, 2016)), in the present work, we focus only on the horizontal and vertical planes. This is because these plans have already been previously evaluated and led to excellent results when used in conjunction with multi-stream architectures in the work developed by Concha et al. (2018).

The presented VR definition is the basis of the WVR. The WVR is the method proposed in the present work to enhance the VR encoding. It is based on the assumption that when the video is being recorded, there is a higher probability that the main action is framed in the central region of the scene. Thus, if we take into consideration the lines around the middle row or column when extracting the VR, it could be a better representation of the performed action. More details about the WVR are given in Chapter 4.

3 RELATED WORK

HAR methods can be divided into two types: hand-crafted and automatic learning feature-based methods (LIU et al., 2016). The current approaches to learn automatic features are mostly based on DL architectures. These architectures can be viewed as single or multi-stream models. In the present work, both types of features are used together with a multi-stream architecture. Therefore, the following sections comprise a literature review on these topics.

3.1 HAND-CRAFTED FEATURE BASED APPROACHES

Previous to CNN approaches, several authors addressed the video representation problem using hand-crafted features. A typical used fundamental to ground these approaches was to extend notable image descriptors to the video domain. The following paragraphs describe some of these approaches. It is worth mentioning that all cited works (except for the Local Trinary Patterns approach (YEFFET; WOLF, 2009)) used bag-of-features as the final representation and performed the action classification using a Support Vector Machine (SVM) classifier.

Following the commented fundamental of extending image descriptors to videos, Scovanner et al. (2007) introduced the 3D Scale-Invariant Feature Transform (SIFT). SIFT is a method for image feature generation that is invariant to image scaling, translation, and rotation (LOWE, 1999). The 3D SIFT encodes both space and time local information into a descriptor that is robust to orientation changes and noise. Similar to this approach, Willems et al. (2008) presented a scale-invariant spatiotemporal interest points detector. The detected points are described using an extension of the Speeded-Up Robust Features (SURF) descriptor. The SURF descriptor (BAY et al., 2006) was created to be an alternative to the SIFT descriptor, and it also aims to be robust against different image transformations.

Klaser et al. (2008) developed a descriptor based on 3D-gradients applying Histogram of Gradients (HoG) concepts to 3D. HoG is a static image descriptor built from local histograms of image gradient orientations. It was first employed for hand-gesture detection, and later it has become widespread by its application for human detection in images

(DALAL; TRIGGS, 2005). Its 3D version was conceived from the visualization of videos as spatiotemporal volumes. A video is sampled along the three dimensions (X, Y and T) and divided into 3D blocks. The orientations of these blocks are quantized into a histogram which has its bins determined from congruent faces of regular polyhedrons. Klaser et al. (2008) evaluated and optimized the method's parameters for action recognition in videos.

Some works used the classic HoG descriptor as a static feature to complement motion features (DALAL et al., 2006; LAPTEV et al., 2008; WANG et al., 2009, 2013). In these works, one of the motion features used is the Histogram of Optical Flows (HoF). The OF is a pixel motion estimation between consecutive frames by means of a flow field computation (ZACH et al., 2007). As in the HoG construction, the OF orientations are quantized into bins to create the HoF. OF-based descriptors are still used nowadays as a pre-processing step on various DL models, and they are also employed in the present work.

The Motion Boundary Histograms (MBH) was another hand-crafted motion descriptor proposed in the literature (DALAL et al., 2006; WANG et al., 2013). This method is a combination of the two previous descriptors, HoG, and HoF. The MBH is computed from the gradients of the horizontal and vertical components of the OF. This descriptor encodes relative motion between pixels while removes camera motion and keep information about flow field changes. A further improvement on MBH descriptor was proposed in the work of Wang et al. (2013), namely Improved Dense Trajectories (IDT). They proposed to detect camera motion and prune it to keep only trajectories of human and objects of interest. To perform camera motion estimation, the authors detected and tracked feature points between frames using SURF and OF descriptors. Then, they computed the homography using the matched points and the RANdom SAmple Consensus (RANSAC) method. The human motion usually creates inconsistent matches. These inconsistent matches were ignored using a human detector. The estimated camera motion was then canceled from the OFs. The final descriptor was a combination of Trajectory, HoF and MBH computed with warped OF with background trajectories removed and encoded using Fisher Vectors. Although the result of that work is no longer state of the art (SOTA), it is still used as a complementary feature in some DL methods.

Yeffet and Wolf (2009) introduced the Local Trinary Patterns as a 3D version of the

Local Binary Patterns (OJALA et al., 1994). The Local Trinary Pattern is a descriptor that encodes only motion information. Each frame is divided into patches. Then, each pixel of each patch is encoded as a short string of ternary digits, namely "trits". The encoding is based on the similarity of the current pixel compared to the corresponding pixels in the previous and next frames. The histograms of "trits" are computed for each patch, and they are accumulated to represent the frame. The video representation is obtained by the histograms accumulation over the frames (YEFFET; WOLF, 2009).

The majority of these methods was evaluated on small datasets, for instance, KTH (SCHULDT et al., 2004) and Weizmann (BLANK et al., 2005). Hence, the hand-crafted features are extracted regarding specific video sequences of those datasets. This makes the generalization to other real-world scenarios challenging since it is impossible to know which one of them is important for other recognition tasks without retraining (LIU et al., 2016). In contrast, DL methods are capable of extracting generic features from large datasets that can be used on different visual recognition problems (DONAHUE et al., 2014).

3.2 3D-BASED APPROACHES

Since the success of the AlexNet (KRIZHEVSKY et al., 2012) in the image classification problem, CNNs have become SOTA for this task. Since the 3D counterpart of an image is a video, the emergence of methods using 3D CNNs to address the video classification problem was a natural consequence. However, this shift between domains is not trivial. For instance, the transition from 2D to a 3D CNNs implies an exponential increase of parameters, making the network more prone to overfitting. Despite this, some authors created architectures following this reasoning and achieved some impressive results.

Tran et al. (2015) proposed a 3D CNN to learn spatiotemporal features from video datasets. They empirically found that simple $3 \times 3 \times 3$ convolutional kernels are the best option for 3D CNNs, which is similar to findings related to 2D CNNs (SIMONYAN; ZISSERMAN, 2014b). A linear SVM classifier was used within the proposed method. The features of the Convolutional 3D (C3D) network combined with IDT (WANG; SCHMID, 2013) features settled a new SOTA when this work was released. However, their accuracy was outperformed by the two-stream work (WANG et al., 2015b) released later in the same year.

Similar to the Xception image classification network (CHOLLET, 2017), which explores depthwise separable convolutions, the "$R(2+1)D$" (TRAN et al., 2018) explored the same concept for video classification based on 3D CNNs. The "$R(2+1)D$" consisted of a spatiotemporal block of convolution that performed a 2D spatial convolution followed by a 1D temporal convolution with an activation function after each operation. The "$R(2+1)D$" added more nonlinearity if compared to the other approaches, and this is one of the factors that the authors claim to be the reason of the better results. They adapted a Residual Network (ResNet) for their experiments. The authors also experimented heterogeneous networks having the first layers with 3D convolutions and the rest of the network with 2D convolutions. It is interesting to note that the best experimental results achieved on every tested dataset were using a two-stream approach, having as backbone a residual network composed by "$R(2+1)D$" blocks.

Another architecture based on a 3D-like method was the Two-Stream Inflated 3D ConvNet (I3D) (CARREIRA; ZISSERMAN, 2017). The I3D was built upon on the inflation of CNNs by the expansion of kernels to a three-dimensional space. This expansion made the network capable of learning spatiotemporal features. Similar to what was done by Wang et al. (2015b) to bootstrap the input layer weights pre-trained on ImageNet, the inflated layers also took advantage from the ImageNet by copying the weights and rescaling them. The base network was the GoogLeNet (SZEGEDY et al., 2015), also known as Inception-V1. The typical square kernels were transformed into cubic. Except by the first two pooling layers, every other kernel was also extended to pool the temporal dimension. The main contribution of that work was the transfer learning from pre-training on both ImageNet (DENG et al., 2009) and a bigger HAR dataset named Kinetics (KAY et al., 2017). This transfer learning helped to boost performance on other action recognition datasets, UCF101 and HMDB51, establishing new SOTA results on them.

3.3 MULTI-STREAM METHODS

Since Simonyan and Zisserman (2014a) proposed to exploit and merge multiple features, multi-stream methods have been explored and achieved state-of-the-art results on several datasets surpassing hand-crafted methods (WANG et al., 2016a, 2017; CARREIRA; ZISSERMAN, 2017). These approaches were mainly based on having at least one spatial and one temporal stream. That first method showed to be successful, and other extensions

emerged combining more than two streams (FEICHTENHOFER et al., 2017; CHOUTAS et al., 2018; WANG et al., 2018). In the following subsections, some of these approaches are described and compared to the present work. The last subsection comprehends some works that attempted to combine and select features in ways contrasting to what is commonly done in the literature.

3.3.1 Spatial feature based approaches

There are plenty of highly successful CNNs for the image classification problem (SIMONYAN; ZISSERMAN, 2014b; SZEGEDY et al., 2015, 2016; HE et al., 2016). In order to take advantage of such CNNs for the HAR problem, many works have proposed to explore 2D representations of the videos. The static RGB information from video frames was the most adopted feature for this purpose (SIMONYAN; ZISSERMAN, 2014a; WANG et al., 2015b). Static images by themselves are useful indications of movements since some actions are generally accompanied with specific objects (SIMONYAN; ZISSERMAN, 2014a). However, training a CNN from scratch with raw frames from video samples is not the best approach (SIMONYAN; ZISSERMAN, 2014a). It was empirically showed that performing transfer learning from image datasets by fine-tuning a pre-trained network increases HAR performance (SIMONYAN; ZISSERMAN, 2014a). The ImageNet (DENG et al., 2009) is the dataset normally used for this goal.

The original two-stream work of Simonyan and Zisserman (2014a) defined some approaches to deal with the spatial stream. Other authors later adopted these approaches (WANG et al., 2015b; MA et al., 2017). The usage of a slightly modified version of the ClarifaiNet (ZEILER; FERGUS, 2014), called CNN-M-2048 (CHATFIELD et al., 2014), was among these approaches. Since this network requires inputs with a fixed size of 224×224, at the training phase, a sub-image with this size is randomly cropped from a selected frame. The frame is subjected to some data augmentation transformations that will be discussed in Section 3.4. When testing, more than one frame and its augmented crops are used to infer the classification. The final class of a video is obtained by averaging the class scores through all crops. This training protocol, with slight modifications, was later adopted by many works in the literature (WANG et al., 2015a,b; ZHU et al., 2018; FEICHTENHOFER et al., 2017; CARREIRA; ZISSERMAN, 2017; WANG et al., 2018). These works used different CNNs, such as VGG-16 (SIMONYAN; ZISSERMAN,

2014b) and GoogLeNet (SZEGEDY et al., 2015). In the present work, these protocols for training and testing are also employed.

3.3.2 Temporal Feature based approaches

Even multiple frames are not able to capture the correlation between movements along time and fail to distinguish similar actions (ZHU et al., 2018). As mentioned earlier, many works employed OF sequences as temporal features to supply the correlations along time and to complement RGB based CNNs (NG et al., 2015; ZHU et al., 2016; WANG et al., 2016a). The two-stream model (SIMONYAN; ZISSERMAN, 2014a) was a pioneer work that successfully applied the OF to videos using the implementation provided by *OpenCV* (BROX et al., 2004). They proposed to stack the OF from L consecutive frames. In their experiments, it was empirically evaluated that $L = 10$ was the best value. Since the horizontal and vertical components of the OF vector fields were computed individually, the employed CNN architecture was modified to have an input layer with 20 channels ($224 \times 224 \times 2L$). The temporal stream by itself outperformed the spatial one, which conferred importance to the specific motion information.

Similar to what happened with the spatial stream, the temporal method proposed in the two-stream work (SIMONYAN; ZISSERMAN, 2014a) was extended in several later works. In Wang et al. (2015b), the 10-frame approach was used on training a temporal network. It is worth mentioning that the features obtained from the OF vector fields are very different from those features obtained from static RGB images. However, they observed that the usage of the ImageNet dataset (DENG et al., 2009) to pre-train the temporal stream can increase its performance. To this end, they discretized the extracted OFs like a RGB image, averaged the weights of the first layer across the channel dimension, and then they copied the average results over the 20 channels of the modified architecture (WANG et al., 2015b). This improved temporal stream is used in this present work and was employed in some other works in the literature (BALLAS et al., 2015; WANG et al., 2016b; DIBA et al., 2017; FEICHTENHOFER et al., 2017).

Derived from the OF definition, the Optical Flow guided Feature (OFF), introduced by Sun et al. (2018), aimed to represent compactly the motion for video action recognition. This method consisted of applying the OF concepts to the difference of feature maps of consecutive frames. Since all the operations in this method are differentiable, the OFF can

be plugged into a CNN architecture fed with RGB frames. This last property granted the OFF the possibility of being trained in an end-to-end manner. One of the main purposes of this work was to avoid the expensive run-time in the classical OF computation. However, this approach only achieved SOTA comparable results when combined with a temporal stream fed with the standard OF feature.

The work of Zhang et al. (2016) enhanced the original two-stream work (SIMONYAN; ZISSERMAN, 2014a) by replacing the input of the temporal stream with motion vectors. Similar to what was done in the work of Fan et al. (2018), the authors aimed to reduce the time expended in the pre-processing step of the temporal stream. The initial idea was to extract the motion vectors directly from the compressed videos and use them as the input for the temporal stream. However, they observed that simply replacing the OF with the motion vectors critically reduced the recognition performance. As a workaround, it was proposed to use three different techniques to transfer learning from a trained OF network to a motion vector CNN. Although this method did not achieved state-of-the-art accuracy, they get high-speed inference time of 391 frames per second (fps) on UCF101.

Also building upon two-stream CNNs (SIMONYAN; ZISSERMAN, 2014a), the Deep networks with Temporal Pyramid Pooling (DTPP) approach was proposed (ZHU et al., 2018). The method consisted of dividing the whole video into T segments of equal length. From each segment, one frame was sampled and used as input to a CNN. The obtained feature vectors were aggregated to form a single video level representation. This aggregation was obtained through a temporal pyramid pooling layer placed at the end of the network. The proposed architecture, which has the BN-Inception CNN (IOFFE; SZEGEDY, 2015) as a backbone network, was trained end-to-end. They explored the number of levels of the pyramid pooling in their experiments, and used a simple average to fuse the streams. For the temporal stream, only five consecutive OF fields were used. With the exploitation of the pre-training using Kinetics (KAY et al., 2017), they were able to set a new SOTA for the HMDB51 dataset.

Although the high performance achieved only by the application of the OF in multi-stream methods, its extraction process is computationally expensive. The *TVNet* was designed in order to avoid this bottleneck (FAN et al., 2018). It is an end-to-end trainable architecture capable of learning OF-like features from datasets. The *TVNet* layers try to mimic the optimization process of the TVL1 method (ZACH et al., 2007). The developed

architecture was coupled with the BN-Inception network (IOFFE; SZEGEDY, 2015) and trained in a multi-task style. The overall loss of the network was set to be a combination of the classification and flow losses. This architecture was able to outperform the classical temporal stream performance. Moreover, they combined the *TVNet* with a spatial stream in order to be competitive with state-of-the-art works. Given the importance of the motion in the two-stream method, in the average combination, the authors weighted the temporal and the spatial streams with 2 and 1, respectively.

Sequences of long-term dependencies are essential to model temporal features. Recurrent Neural Networks (RNNs) and their variants are models capable of learning such long-term dependencies. However, they are still not powerful enough for the video recognition problem. To this end, the *shuttleNet* Deep Neural Network (DNN) was proposed (SHI et al., 2017). It was inspired by feedforward and feedback connections of the biological neural system. The *shuttleNet* topology was composed of D groups with N processors structured as rings. Each processor was a Gated Recurrent Unit (GRU) (CHO et al., 2014). The final architecture was constituted of a two-stream model, which extracted the deep features to be used as input for the *shuttleNet*. Besides that, they used only a single OF as the input of the temporal stream. It was showed in the experiments that the *shuttleNet* performed better than other RNNs. To further improve their results, the authors late-fused the final results with a descriptor called Multi-skIp Feature Stacking (MIFS) (LAN et al., 2015).

The Temporal Segment Networks (TSN) was built upon on the successful two-stream architecture (SIMONYAN; ZISSERMAN, 2014a) and aimed for modeling long-range temporal structures (WANG et al., 2016a). Besides the two commonly used information on multi-stream models, RGB frames and stacked OF fields, other two types of inputs are empirically explored to feed the network, namely stacked RGB difference and stacked warped OF fields. Utilizing a sparse sampling scheme, short clips were obtained from video samples, and they were used as the input of the TSN. A segmental consensus function yielded the final prediction. They observed that the best results of TSN were obtained when the classical RGB and OF features were combined with the proposed warped OF features. In additional experiments, the authors also observed that the best segmental consensus function was average pooling (max and weighted were also tested) and the best backbone network for the architecture was the BN-Inception (ClarifaiNet, GoogLeNet, and VGG-16 were also tested).

The work of Song et al. (2019) introduced the operation named Temporal-Spatial Mapping (TSM). The TSM captures the temporal evolution of the frames and build a 2D feature representation, called *VideoMap*, which combines the convolutional features of all frames into a 2D feature map. The convolutional features were extracted using the same procedure adopted by (WANG et al., 2016a) to extract deep features.

3.3.3 Spatiotemporal feature based approaches

Despite the success achieved by multiple stream methods, they have the problem of not allowing communication between the streams (SIMONYAN; ZISSERMAN, 2014a,b; NG et al., 2015; WANG et al., 2016a). This lack of interaction hinders the models from learning spatiotemporal features that may be crucial to learn some tasks (KONG; FU, 2018). Different methods were proposed to extract such features. Some of these approaches are briefly described below.

Diba et al. (2017) presented a video representation, the Temporal Linear Encoding (TLE). Inspired by the work of Wang and Schmid (2013), the TLE was a compact spatial and temporal aggregation of features extracted from the entire video, which was used in an end-to-end training. Two approaches of extraction and two approaches for TLE aggregation were experimented: two-stream CNNs (as in Wang et al. (2015b)) and the C3D network (TRAN et al., 2015) for extraction, and bilinear models and fully-connected polling for aggregation. They discovered that the two-stream extraction method (using the BN-Inception (IOFFE; SZEGEDY, 2015) as backbone network) and the bilinear aggregation method (PHAM; PAGH, 2013; GAO et al., 2016) yielded better results on both UCF101 and HMDB51 datasets.

Wang et al. (2017a) proposed to exploit jointly spatiotemporal cues by using a spatiotemporal pyramid architecture, which can be trained in an end-to-end manner. It was argued that using only ten consecutive OF frames may lead to misclassification between two actions that could be distinguished in the long term. Therefore, they used multiple CNNs with shared network parameters but with different OF chunks of the same video sample as input. Moreover, the authors proposed a bilinear fusion operator named Spatiotemporal Compact Bilinear (STCB). The STCB was used to create the final representation of the temporal stream and to merge the two streams with an additional attention stream. In their experiments, they discovered that BN-Inception was the best

base architecture for both spatial and temporal streams.

The Eigen Evolution Pooling (EEP) was created aiming to obtain a spatiotemporal representation of videos (WANG et al., 2017b). It was based on the concept of representing a sequence of feature vectors as an ordered set of one-dimensional functions. This representation, extracted directly from the RGB frames, became the input of a CNN. The EEP performed better than other comparable pooling methods, *e.g.*, dynamic images. In order to complement the experiments, the EEP was applied to the TSN features and then combined with IDT (WANG; SCHMID, 2013) and VideoDarwin (FERNANDO et al., 2015) hand-crafted features. This last experiment showed that this method is comparable to the state-of-the-art approaches.

Spatiotemporal features can be obtained when there is some data transfer between the spatial and temporal streams of an architecture. To this end, Feichtenhofer et al. (2017) proposed interactions between streams. The residual connections originated from the ResNets inspired the connections linking the streams. Besides the additive interaction present on the ResNets, they proposed the multiplicative interaction to compose the Spatiotemporal Residual Networks (ST-ResNets) architecture (FEICHTENHOFER et al., 2016). This last one showed to be more efficient than the additive interaction. Additionally, the authors verified an accuracy improvement when merging this method with IDT features.

Choutas et al. (2018) proposed a representation, named Pose moTion (PoTion), to encode motion of some video key points. In every frame, heatmaps for human joints were acquired by human pose estimation. These heatmaps were colorized according to their position in time. Then, the heatmaps were summed to obtain the final PoTion representation, which has the same dimensions as a single frame. This representation was the input of a shallower CNN (with seven layers) that predicts the final class. The PoTion representation alone was not able to achieve good results. However, the authors combined it with the I3D multi-stream (CARREIRA; ZISSERMAN, 2017) which slightly improved the state-of-the-art accuracy on the UCF101 dataset.

3.3.4 Other approaches

A way to achieve better results is combining existent features with new ones. In this context, each stream can be interpreted as an expert. Based on this key idea, the Product

of Experts (PoE) was proposed (SENGUPTA; QIAN, 2017). The PoE was applied to a four-stream architecture named pillar networks derived from works of Wang et al. (2016a); Ma et al. (2017). They extracted convolutional features from spatial and temporal streams using the BN-Inception network (IOFFE; SZEGEDY, 2015) and from spatial and temporal using the ResNet-101 (HE et al., 2016). The authors divided the training set of the HMDB51 into seven non-overlapping groups. Each stream was trained with each group, thus obtaining 28 experts. When combined, these feature vectors were able to increase individual performance significantly.

A different pooling method was presented by Wang et al. (2018). It was based on the assumption that among the deep features generated by a DL method, there is at least one feature that discriminates the action. In order to find it, they proposed to learn a hyperplane that isolates this feature from the others. The decision boundary was determined using an SVM classifier which was fed with the features extracted from distinct layers of a two-stream architecture. They achieved results comparable to SOTA only when combined with I3D approach pre-trained with the Kinetics dataset (CARREIRA; ZISSERMAN, 2017).

Different from all already mentioned works, the work of Feichtenhofer et al. (2016) focus on answering some questions. For instance, how to fuse two networks (temporal and spatial) taking account of spatial registration and where to fuse them. For the first question, five fusion methods, namely sum, max, concatenation, convolutional, and bilinear, were investigated. For the second question, the authors investigated how fusion behave at different layers. The authors reported that the convolutional fusion at the ReLU5 layer of the CNN-M-2048 network achieved the best results. Fusions at earlier layers showed to have weaker performance. They also merged their features with the IDT hand-crafted features to increase the final performance.

3.4 DATA AUGMENTATION

It is widely known that any NN model with a massive number of parameters is susceptible to overfitting. In order to reduce such high bias, a commonly adopted practice is to increase the amount of data (KRIZHEVSKY et al., 2012). However, sometimes it is hard to gather a satisfactory volume of samples. In this scenario, data augmentation plays a crucial role to enhance DL performance. Data augmentation is a regularization technique

that enlarges datasets and enables the generation of new data samples by applying label-preserving transformations to the dataset (KRIZHEVSKY et al., 2012).

In the context of multi-stream video classification, data augmentation is often applied to the spatial stream inputs. Typical image augmentation techniques are generally applied to these inputs. In the precursory two-stream work (SIMONYAN; ZISSERMAN, 2014a), at the training phase, a randomly selected frame was rescaled to have the smallest dimension equals to 256. From this frame, a sub-image matching the employed network input dimension was randomly cropped. Additionally, this crop was subjected to a random horizontal flipping and RGB jittering. At inference time on the testing set, 25 frames evenly spaced were taken and then augmented 10 times by cropping and flipping the four corners and the center of the frames. This last strategy was adapted in the work of Wang et al. (2015b) for the training phase. The authors argued that the random cropping strategy was more prone to overfit since it was more likely to select regions close to the image center. Hence, they used the 4 corners and the center of the image to increase input variations. In this same work, Wang et al. (2015b) also proposed a multi-scale cropping method. It consisted of resizing the frame to 256×340 and randomly sample the cropping width and height from $\{256, 224, 192, 168\}$. After that, the crop was rescaled to match the network input dimension. These data augmentation methods showed to be very helpful to prevent the overfitting problem (WANG et al., 2015b).

The Multiple Dynamic Images (MDI) was projected as a data augmentation method to overcome the problem of training a network with dynamic images from scratch (BILEN et al., 2016). The dynamic image was an attempt to create a compact video representation to be used as a temporal feature (BILEN et al., 2016). Similar to the VR approach presented in the present work, the dynamic image was a still image representation of the entire video, summarizing its appearance and motion dynamics. The dynamic image was obtained through the application of a rank pooling operation in the video, resulting in a vector with the same dimensions of a single frame. The authors affirmed that there is a large domain gap between dynamic images and natural images, which does not allow a pre-train with the ImageNet dataset. For this reason, it was necessary to increase the number of samples to train a network from scratch. The MDI were proposed to enlarge the number of training samples by extracting multiple overlapping segments of duration τ and with stride s. The MDI approach showed to be better than the single dynamic

image approach.

This MDI approach is particularly similar to the data augmentation used in the present work to extract multiple crops from the SEVR. In this extraction, we experiment different values for the stride s with a fixed length for the crops. Based on the findings of Wang et al. (2015b), we choose to use fixed locations for the crops instead of randomly selecting their positions. These details are discussed in Chapter 5.

4 PROPOSED METHOD

The proposed method is divided into two parts, both aiming action recognition in videos. The first one consists of the presentation of a new approach of VR extraction dubbed WVR. Additionally, we also defined a specific data augmentation method for the VR named symmetric extension. Throughout this chapter ways to explore this data augmentation method for the HAR problem are presented. The second part of the proposed method consists of the usage of both horizontal and vertical WVR, as well as its augmentations, as new spatiotemporal streams. To this end, these streams are used together with the spatial and temporal streams, respectively RGB frames and OF, in a multi-stream architecture as illustrated by Figure 4.1. We expect that the VR could be complementary to the other streams because of its distinct nature that merges temporal and spatial features. To this end, we propose a new method for extracting the Visual Rhythm (VR) named Weighted Visual Rhythm (WVR). Two instances of the WVR, depicted in purple in the Figure 4.1, are employed as spatiotemporal streams.

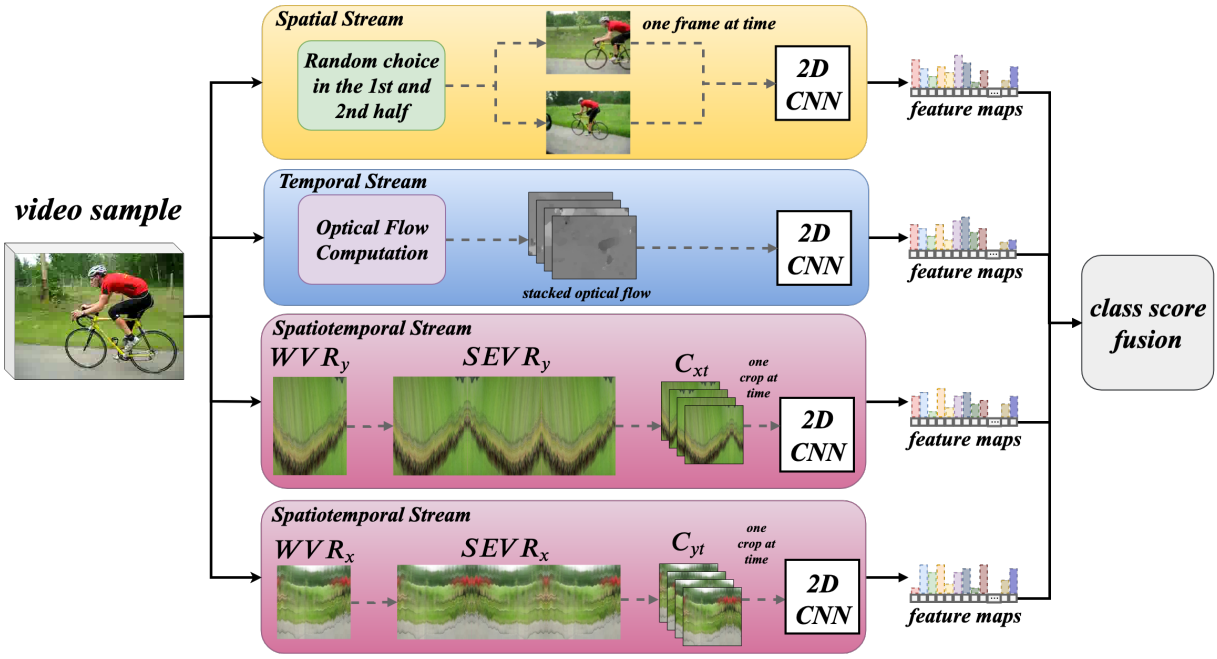

Figure 4.1: Final multi-stream architecture. The training of each stream is performed individually, and a weighted sum of the feature maps determines a descriptor utilized in the final classification.

4.1 WEIGHTED VISUAL RHYTHM

The proposals of Concha et al. (2018) and Souza (2018) that take the mean VR formed by all rows or columns, was adapted. In that proposal, the VR was extracted by taking the mean color value of the frames across the horizontal or vertical direction. By weighting the scene elements far from the main object's or actor's location as the closest ones, one might hinder the motion representation. It is expected that the main events recorded in the video have been framed in its central region. Thus, the underlying moving object or person in a video is more likely to be observed far from the frame borders. Instead of the homogeneous weighting, we propose to weight less as the pixels get farther from a reference row or column. Taking these premises into account and the VR definition of Chapter 2, we defined the WVR as follows. Let $P_r = \{(r,1),(r,2),\cdots,(r,w)\}$ be the set of points forming the row r. We define the horizontal WVR as:

$$\mathrm{WVR}_y = \sum_{r=1}^{h} VR_{P_r} \cdot g(r-y,\sigma_y) \cdot \left[\sum_{r=1}^{h} g(r-y,\sigma_y)\right]^{-1}, \tag{4.1}$$

where y is the reference row of the horizontal VR and $g(s,\sigma) = e^{-\frac{s^2}{\sigma^2}}$ is the weighting function that decays as the other VRs get farther from the reference row y. Conversely, the vertical WVR can be defined in the same way. Let $P_c = \{(1,c),(2,c),\cdots,(h,c)\}$ be the set of points forming the column c. We define the vertical WVR as:

$$\mathrm{WVR}_x = \sum_{c=1}^{w} VR_{P_c} \cdot g(c-x,\sigma_x) \cdot \left[\sum_{c=1}^{w} g(c-x,\sigma_x)\right]^{-1}, \tag{4.2}$$

where x is the reference column of the vertical VR and $g(s,\sigma) = e^{-\frac{s^2}{\sigma^2}}$ is again the weighting function that in this case decays as the other VRs get farther from the reference column x. Thus, the WVRs used in the present work are defined by two parameters: the reference row y and standard deviation σ_y, for the horizontal version; and the reference column x and standard deviation σ_x, for the vertical one. In practice, some simplifications are adopted. An interval $y \pm d_y$ is defined from σ_y such that outer rows have zero weight. Furthermore, to make the parameter y invariant to video height h, we define a factor α_y such that $y = \alpha_y \cdot h$. Those same simplifications also apply for the vertical VRs. An interval $x \pm d_x$ is defined from σ_x such that outer columns have zero weight, and the α_y factor is defined as $x = \alpha_x \cdot w$ to make the x parameter invariant to the video width w.

Figure 4.2 (a) depicts a video of the *biking* class from the UCF101 dataset (240 frames with 320 × 240 pixels), forming a horizontal WVR of 320 × 240 elements and Figure 4.2 (b) depicts the same video forming a vertical WVR of 240 × 240 pixels.

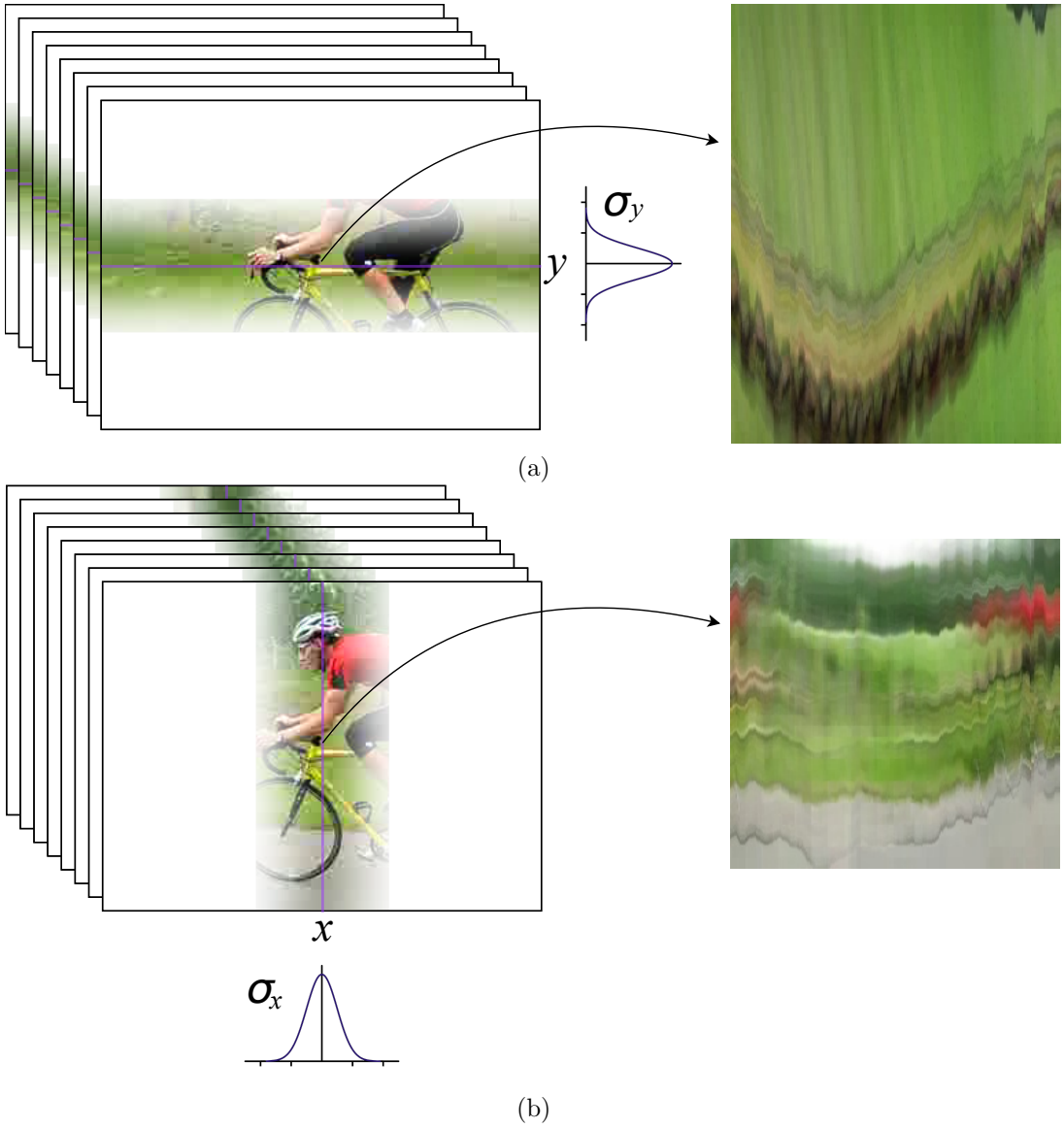

Figure 4.2: Weighted Visual Rhythm of a sample video of the class *biking* from UCF101 dataset: y is the middle row in the horizontal rhythm (a), and x is the middle column in the vertical rhythm (b), and σ_x and σ_y are both equal to 33.

Notice that the WVR can be seen as a middle term between the simple VR defined in Chapter 2 and the VR used by Concha et al. (2018) that takes the mean across all rows or columns. In the extreme case, when σ_y or σ_x assumes large values, the WVR has no distinction if compared to the mean VR. Figure 4.3 illustrates such comparisons using the same video from the previous examples. Although the work of Concha et al. (2018) had extracted the VR from the black and white version of the videos, here we also make the

comparison with the colored version of it. The WVR tends to show smoother patterns in contrast to the simple VR. This is due to the weighting function that is equivalent to a Gaussian filter which attenuates the high frequencies in the images (GONZALEZ; WINTZ, 1987). Therefore, the VR is equivalent to a video sampling, and the usage of a Gaussian weighting function is the most effective low pass filter avoiding aliasing during the process of VR extraction. Other functions could be explored for the weighing process. However, we do not analyze this question in the present work.

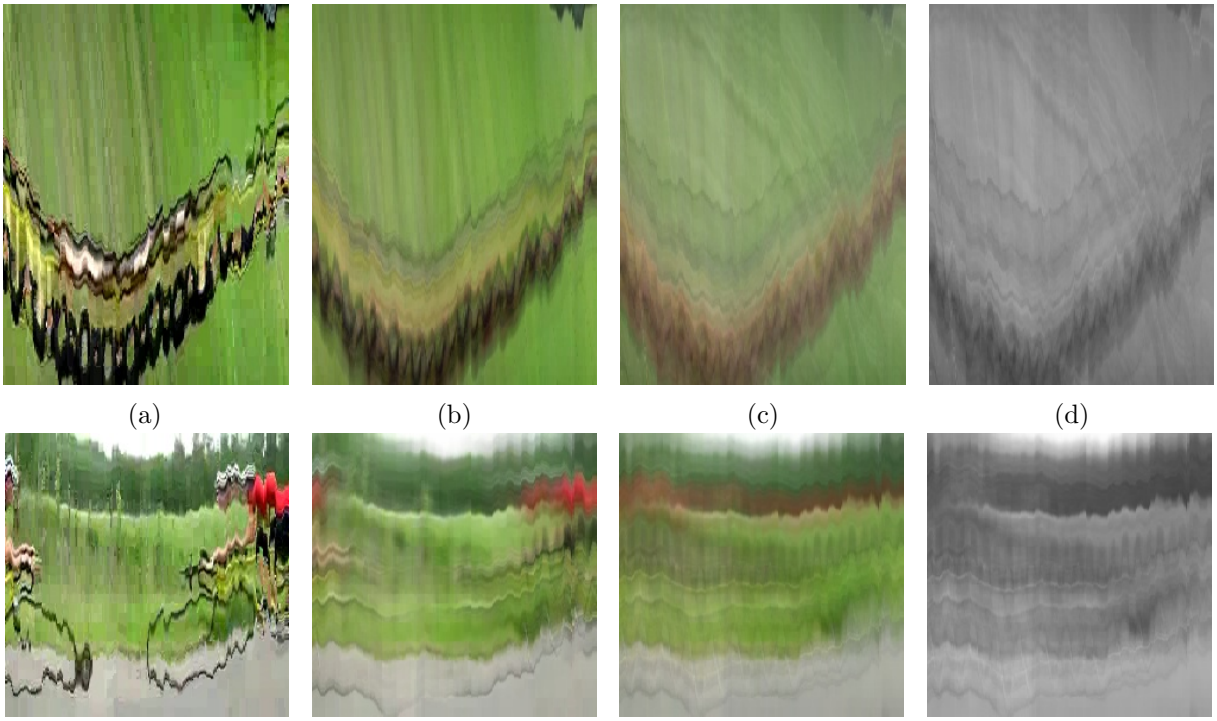

Figure 4.3: Different Visual Rhythm versions of the same video sample of the class *biking* from UCF101 dataset. First row (a-d) consists of the horizontal versions and the second one (e-h) consists of the vertical versions. From left to right: simple Visual Rhythm, Weighted Visual Rhythm, and mean Visual Rhythm colored and in grayscale. The simple rhythms used the middle row and column as reference lines, and the weighted rhythms used $\alpha_x = \alpha_y = 0.5$ and $\sigma_x = \sigma_y = 33$.

Through the VR images of the Figure 4.3, it is possible to notice that in the mean rhythm (c, g) the formed patterns tend to become a little more scattered in contrast to the more concentrated patterns in the other two approaches (a-b, e-f). When using the average of the frames, the colors of formed pattern tend to be slightly distorted of the colors of the element that originated those patterns. For example, the black pattern formed by the cyclist's shorts (a-b) is depicted in brown in the mean rhythm (c). This is probably because of the green background blending of that video, which is another

point to highlight. The green color covering a large area of these generated rhythms is a strong indication that the action portrayed is performed outdoors. This information can be useful to restrict classification to actions that are normally performed outdoors. This type of information is impossible to obtain using grayscale rhythms (d, h). However, these observations are based on only one video sample and do not assess the superiority of one approach over another. To investigate the real impact of using one VR over another, in Chapter 5 we explore the sigma parameters σ_y and σ_x. High accuracy with a little value of sigma would be indicative in favor of the simple VR, and the extreme opposite would favor the mean rhythm. However, we expect that a median value for sigma achieve the best results and corroborate to our hypothesis that the central region contains more relevant information for HAR in videos.

4.2 SYMMETRIC EXTENSION

As stated in Section 3.4, data augmentation is an important method to increase the number of data samples available to train a DL architecture and, consequently, increase performance. In CV context, data augmentation consists of applying label-preserving transformations to original samples presented in a dataset to obtain new samples (FAWZI et al., 2016).

Since the VR can be interpreted as an image, one could propose to employ standard techniques of image data augmentation. However, the temporal nature of one of its dimensions demands some cautions. A rescaling transformation, for instance, would be equivalent to modify the sample rate of the original video. To illustrate this case, Figure 4.4 shows the effects of up-sampling two VRs, one from the class *run* (a) and another from the class *walk* (b), both from the HMDB51 dataset. In these VRs, inclined thin lines depict the main pattern of both actions (highlighted in yellow rectangles). An obvious distinction between these patterns is the inclination angle, which becomes less prominent after the transformations in both images. This is due to the video sample of the *run* class has only a few frames. Thus, resizing dilates the action pattern along the time dimension. This distortion would not be a problem if the transformation could be applied homogeneously to all samples. But, since each video has a different duration, this is not possible.

When using VRs, the described situation turns to a problem considering that some video samples does not have enough frames to reach the required input dimension of

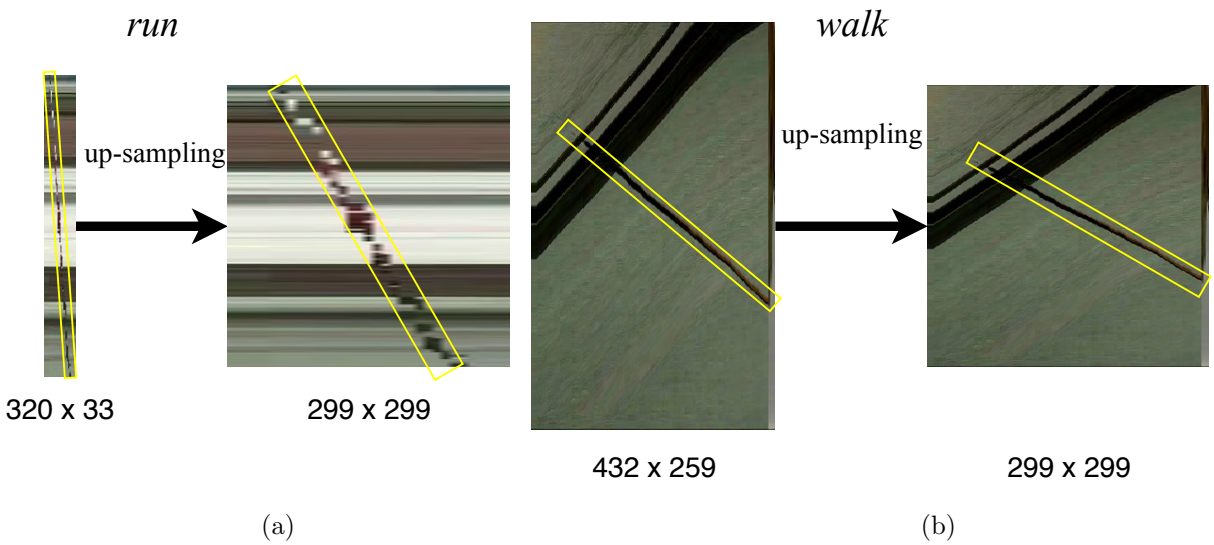

Figure 4.4: Up-sampling of two different Visual Rhythms from HMDB51 dataset. The yellow rectangles highlight the main action pattern of each rhythm. Notice that, after the transformation, the angles of inclination of each action pattern become closer to each other in contrast to the obvious distinction between them previously.

the employed network (299×299 for InceptionV3). Concha et al. (2018) proposed to handle this question by repeating the video frames from the beginning until they reach the necessary amount of frames. However, this approach creates abrupt discontinuities in the VR that could harm the recognition. Instead of doing this, in the present work, we propose to repeat the frames backward in time, avoiding sudden cuts, and creating a symmetric extension for the VR. The symmetric extension of a horizontal WVR is defined as:

$$\mathrm{SEVR}_y(i,k) = \begin{cases} \mathrm{WVR}_y(i, f-m), & \text{for } \lfloor k/f \rfloor \text{ odd} \\ \mathrm{WVR}_y(i, m+1), & \text{otherwise} \end{cases} \tag{4.3}$$

where $1 \leq i \leq w$, m is the remainder of the integer division of k by f and $k \in \mathbb{Z}$. Analogously, the symmetric extension of a vertical WVR is defined as:

$$\mathrm{SEVR}_x(i,k) = \begin{cases} \mathrm{WVR}_x(i, f-m), & \text{for } \lfloor k/f \rfloor \text{ odd} \\ \mathrm{WVR}_x(i, m+1), & \text{otherwise} \end{cases} \tag{4.4}$$

where $1 \leq i \leq h$, m is the remainder of the integer division of k by f and $k \in \mathbb{Z}$. Thus, the SEVR is composed of several copies of the VR concatenated several times along the temporal dimension with the even occurrences being horizontally flipped. Figure 4.5

shows both horizontal (a) and vertical (b) WVRs of a video of the *biking* class of UCF101 extended three times. The premise is as follows: we observed that symmetrical gestures constitute the majority of actions, e.g. *typing*, *brushing teeth*, *drumming*, *pull ups*, *playing guitar*, etc. Thus, the action performed backward in time also represents the class and can be used to reinforce the CNN training. The symmetric extension circumvents the temporal limitation of videos and turns feasible the application of some data augmentation methods.

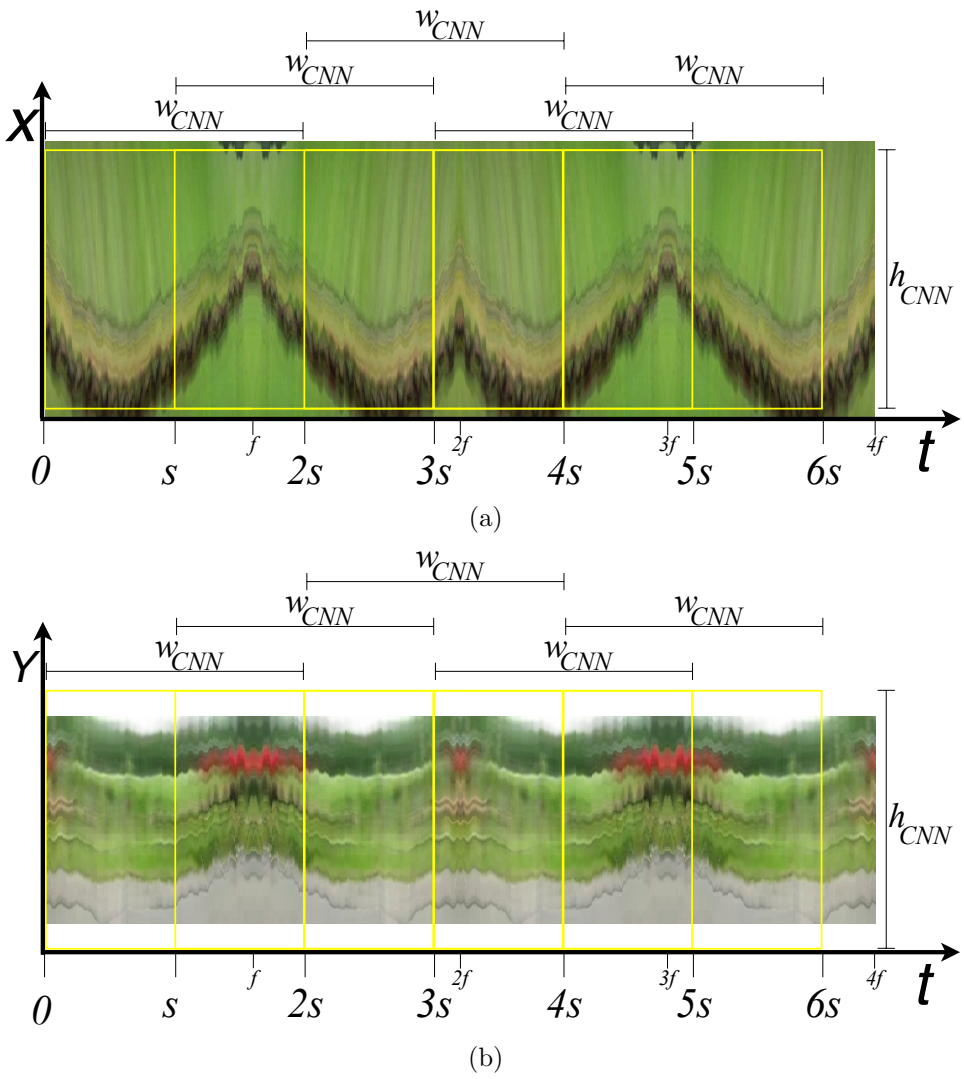

Figure 4.5: Extraction of five squared crops from the symmetric extensions of both horizontal (a) and vertical (b) Visual Rhythms of the same video of the class *biking* from UCF101 dataset. The frame width is $w = 320$ pixels, the frame height is $h = 240$ pixels, and the corresponding video length is $f = 240$ frames. The stride between crops is $s = 150$ pixels and the crop dimensions are $w_{CNN} = h_{CNN} = 299$. The central area in X is selected in (a) and in (b) the rhythm will be stretched in Y to cover the crop dimensions.

4.2.1 Symmetric Extension with Fixed Stride Crops

With the SEVRs, it is possible to obtain crops to match the required input dimension of the employed network. We propose to go further and extract more than one crop per video and, consequently, augmenting the available data. The observation that supports this idea is that long duration video samples usually exhibit the action more than once. The symmetric extension allows short video samples to share this same behavior. Hence, a crop would possibly contain a full cycle of the action, even being only a fraction of the entire VR or the SEVR.

We propose to use multiple crops from each extended VR as a data augmentation process. Each crop is formed by the image constrained in a window of dimensions $w_{CNN} \times h_{CNN}$ (matching the CNN's input). A crop C_{xt} from the horizontal SEVR with lower left coordinates x and t is defined as:

$$\mathrm{C}_{xt}(a, b) = \mathrm{SEVR}_y(x + a, t + b), \tag{4.5}$$

with $x \leq a < x + h_{CNN}$ and $t \leq b < t + w_{CNN}$. And a crop C_{yt} from the vertical SEVR with lower left coordinates y and t is defined as:

$$\mathrm{C}_{yt}(a, b) = \mathrm{SEVR}_x(y + a, t + b), \tag{4.6}$$

with $y \leq a < y + h_{CNN}$ and $t \leq b < t + w_{CNN}$. The VR is extended symmetrically until n_c crops are extracted using a stride s, i.e., the first crop is taken at $t = 0$ and all subsequent $n_c - 1$ crops are taken s frames ahead the previous one. The resulting set of crops for a fixed row x is $\{C_{xt} \mid t = js\}$, for $j \in \{0, 1, ..., n_c - 1\}$, and similarly, the resulting set of crops for a fixed column y is $\{C_{yt} \mid t = js\}$, for $j \in \{0, 1, ..., n_c - 1\}$.

If h_{CNN} is smaller than the spatial dimension of the SEVR, i.e., the video frame width or height is greater than the corresponding dimension of the CNN, the crops are centered in the spatial dimension. Figure 4.5 (a) depicts this case for the SEVR_y. This approach assumes that the main action motion is mostly performed in these central regions. Notice that the crops do not reach the top and bottom sides. To include these regions, extra n_c crops keeping the stride s from each other are obtained, aligned with the top and bottom borders. Thus, up to $3 \cdot n_c$ crops can be obtained depending on the application. This is useful to get all information in X and for most videos reinforce the central information.

Now, if h_{CNN} is bigger than the spatial dimension of the SEVR, i.e., the video frame width or height is smaller than the corresponding dimension of the CNN, the crops are stretched in the spatial dimension to satisfy the network's input size. Figure 4.5 (b) depicts this case for the SEVR_x. The stride used in Figure 4.5 is only used for illustration purposes.

There is no guarantee that a complete cycle of the action is portrayed in a single crop since we do not have any information about its commencement and conclusion in a video sample. This is another reason to use multiple crops. The probability of getting at least one complete cycle of action increases proportionally with the number of excerpted crops. Besides that, the stride could be helpful for this purpose. This parameter is an attempt to adjust the temporal limits of the crop, aiming to comprehend a full action cycle. To this end, in Chapter 5, we empirically explore distinct values for the stride s together with multiple crops.

4.3 SPATIOTEMPORAL STREAM CLASSIFICATION PROTOCOL

An overview of the proposed method for a spatiotemporal stream using WVRs is depicted in Figure 4.6. It consists of a testing classification protocol using a version of the InceptionV3 network (SZEGEDY et al., 2016) with WVRs. This overview applies to both horizontal and vertical rhythms, but they are explored separately. Thus, two NNs are trained independently.

A WVR is computed for each video, and its data augmentation is driven by symmetric extension. Multiple crops with fixed stride are extracted from the symmetric extension. At the inference time and for video classification, all the augmented crops are individually applied to the CNN, and their last layer feature maps are extracted (just before softmax classification) and averaged. We observed that fusing the feature maps before the softmax normalization, as performed by Diba et al. (2017) and Zhu et al. (2018), achieves better results. A softmax classification layer is applied to this average feature map. The softmax is a function that takes as input a vector of real numbers of dimension N and normalizes it into a probability distribution consisting of N probabilities. The ideal classifier would have 1 in the index correspondent to the correct class and zero in the other positions. The final class prediction is the averaged prediction of all crops.

We argue that this process might yield better class predictions based on the assumption that multiple crops taken at different time positions are representative of a distinct portion

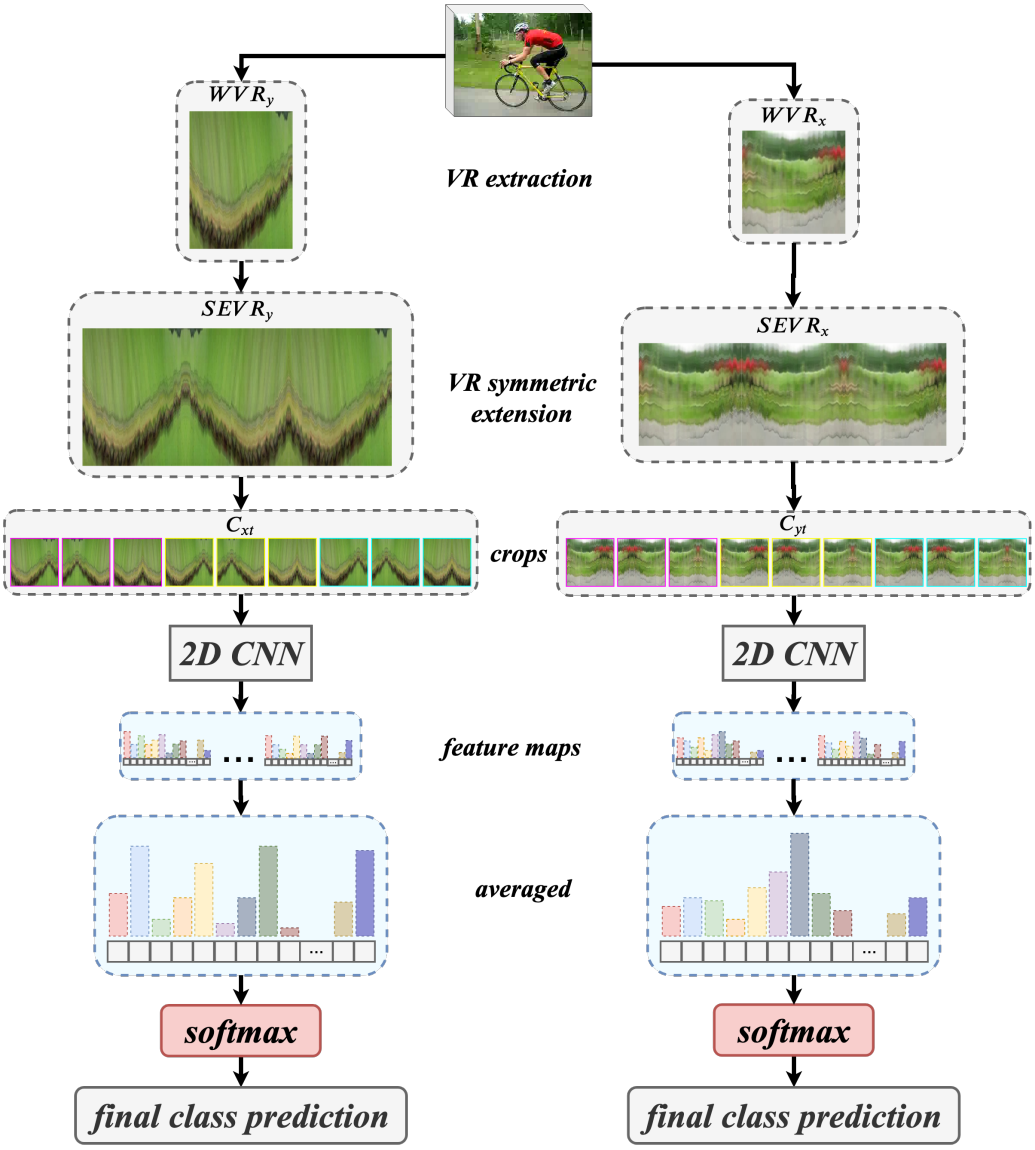

Figure 4.6: Overview of the proposed Visual Rhythm stream. After the symmetric extension, n_c crops apart from each other by a stride s are extracted in the center (yellow). Depending on the dataset, extra crops aligned with the image top (magenta) and bottom (cyan) are extracted. All crops are applied to the CNN. The resulting features are averaged, and the final class is predicted through a softmax layer.

of the underlying action in the video. In the training stage, however, each crop is processed as a distinct sample and separately classified, i.e., the average is not taken into account. The WVR parameters, as well as the SEVR parameters, are explored in Chapter 5 using the described spatiotemporal stream and classification protocol.

4.4 MULTI-STREAM CLASSIFICATION PROTOCOL

Two instances of the spatiotemporal stream, one operating on horizontal WVRs and another operating on vertical WVRs, are used together with the already discussed spatial and temporal streams to form a multi-stream architecture. In the overview of the proposed multi-stream architecture, depicted in Figure 4.1, the spatiotemporal streams are represented in purple, and the spatial and temporal streams, already explained in Sections 2.4 and 2.5, are represented in orange and blue, respectively.

Each stream is trained individually, and all of them use a version of the InceptionV3 network pre-trained with ImageNet. The following details concern to both UCF101 and HMDB51 datasets. We adopt the improved spatial stream described by Concha et al. (2018) as well as the training and testing protocols used in that work. More specifically, in this stream, two random frames per video, one from each half of the video, are used as a representation of each sample in the training phase. In the testing phase, 25 frames are taken uniformly over the video length. The CNN receives one frame at a time in both phases. We use the multi-crop augmentation with horizontal flips proposed by Wang et al. (2015b). Thus the test prediction is performed by averaging 250 feature maps.

For the temporal stream, a stack of 10 consecutive OFs, extracted from a random initial position in the video, fed the network. Hence, the input has 20 channels since the OF is decomposed into horizontal and vertical components. The stack size is based on the results of Simonyan and Zisserman (2014a) and Wang et al. (2015b).

The testing phase of the temporal stream is very similar to the spatial stream: a stack of 25 evenly sampled OFs and its augmentations obtained through multi-crop and horizontal flip transformations are employed together to classify the video. The spatiotemporal streams in this multi-stream architecture follow the training and testing protocols described in the previous section.

A fusion of the feature maps of each stream produces the final classification for the multi-stream architecture. This fusion is a weighted sum of the feature maps. A grid search strategy is used to find out the best weights.

The feature maps used for this are also extracted before the application of the softmax. Section 5.2 gives implementation details about both spatiotemporal stream and multi-stream architectures.

5 EXPERIMENTAL RESULTS

In this chapter, we evaluate the proposed methods: WVR and SEVR, and the multi-stream architecture using SEVRs. The spatiotemporal stream is assessed by exploring different values for some parameters. It is possible to note that, with a particular set of parameters, a significant performance increase can be achieved for the WVR stream if compared to the baseline. Furthermore, to make our results more competitive and to show the complementarity of the spatiotemporal streams, we explore the multi-stream classification using every possible combination between the employed streams: horizontal WVR, vertical WVR, static RGB frames, and OF.

5.1 DATASETS

The proposed method was evaluated through experiments performed on two challenging video action datasets: UCF101 (SOOMRO et al., 2012) and HMDB51 (KUEHNE et al., 2013).

The UCF101 dataset contains 13320 videos. All videos have a fixed frame rate and resolution of 25 FPS and 320×240 pixels, respectively. This dataset covers a broad scope of actions from the simplest to the most complex ones. An example of the latter is playing some sport or playing some instrument. These videos were collected from YouTube and divided into 101 classes. Since multiple users uploaded them, there is a great diversity in terms of variations in camera motion, object appearance and pose, object scale, and viewpoint. This diversity is essential to replicate the variety of actions that a realistic scenario can have.

HMDB51 is an action recognition dataset containing 6766 videos with 51 different action classes. The HMDB51 includes a wide variety of samples collected from various sources, including blurred videos, or with low quality, and actions performed in distinct viewpoints. Most videos of this dataset originate from movies and a small fraction from public databases, such as the Prelinger archive, YouTube, and Google videos. There is no fixed resolution for the HMDB51 videos.

The evaluation protocol used for both datasets is the same. The average accuracy of the three training/testing splits available for both datasets is reported as the final result.

5.2 IMPLEMENTATION DETAILS

All the code was implemented with Python programming language. For the spatial and temporal stream parts of the multi-stream architecture, we used the implementation of the "Multi-Stream Convolutional Neural Networks for Action Recognition in Video Sequences Based on Adaptive Visual Rhythms" (CONCHA et al., 2018) available on GitHub[1]. In the present work, as well as in Wang et al. (2015b), the authors utilized the TVL1 method (ZACH et al., 2007) for the OF extraction. More specifically, the implementation present in the OpenCV library.

The WVR computation is carried out in two steps, which are applied to each video frame. The application of a 1D Gaussian filter, implemented in the *SciPy* Python module[2], and the extraction of the reference row or column from the frame. Remember that the rows outside the interval $y \pm d_y$ have zero weight what implies that the total width of the employed filter will be $2 \cdot d_y$. The filter width defines the area within which elements will influence the calculation of the WVR. We empirically fixed the d_y value (equivalent to the *truncate* parameter in the *SciPy* implementation) to be $1.5 \cdot \sigma_y$. Thus, the filter spans a total width of $3 \cdot \sigma_y$ and covers approximately 87% of the values of the normal distribution. This also applies to the vertical rhythm and the d_x, σ_x and x parameters. Since we are interested in verifying which portion of the frame most motion are performed, this fixed value fits our purposes. The Gaussian filter was applied only across the corresponding axis of rhythm direction in question, i.e., the filter was applied to the Y axis of the frame when extracting the horizontal rhythm and to the X axis when extracting the vertical rhythm. The OF and WVR extractions were performed as pre-processing steps.

The Keras framework (CHOLLET et al., 2015) was used for all experiments concerning to the spatiotemporal streams. A slightly modified version of the InceptionV3 network (SZEGEDY et al., 2016) initialized with ImageNet (DENG et al., 2009) weights was used in the experiments of Sections 5.3 and 5.4. The InceptionV3 was modified to have an additional fully connected layer with 1024 neurons and 60% of dropout. The softmax classifier was adapted to match the number of classes in each dataset.

All training parameters were kept the same for both datasets. Some Keras random data augmentation approaches (horizontal flip, vertical flip, and zoom in the range of

[1]https://github.com/darwinTC/Adaptive-Visual-Rhythms-for-Action-Recognition

[2]https://docs.scipy.org/doc/scipy-0.15.1/reference/generated/scipy.ndimage.filters.gaussian_filter1d.html

0.8 to 1.2) were applied to the input images. These augmentations were performed in runtime by the framework while the fixed stride crop augmentation, described in Section 4.2, was performed previously as a pre-processing step. We show in Section 5.5 that these data augmentations drive to a significant accuracy increase.The mean RGB values were centered in zero and normalized. To this end, the Wedford's methods of mean and standard deviation accumulative computation (WELFORD, 1962) were incorporated into the Keras framework. This method was used to take advantage of the framework ability to work with batches of data and save memory. The network was trained with the following parameters: learning rate of $1e^{-3}$, batch size of 16, Stochastic Gradient Descent (SGD) optimizer with momentum of 0.9 and categorical cross entropy loss function. The early stop training strategy was adopted with patience of 6 epochs. The learning rate was also scaled down by a factor of 10 after 3 epochs without any improvement in the loss function. The learning rate minimum value was limited to $1e^{-6}$.

Various machines were used in the experiments. The implementation of the WVR extraction was CPU-bound while all DL architectures took advantage of GPU processing. The machine used for the WVR extraction has an Intel® Xeon® E5-4607 processor with 48 threads and 32GB of RAM. Our code was designed to work in a parallel manner and extract the VR of one video per thread available in the machine. Among the machines used for DL architecture training, the following graphic cards were used individually: NVIDIA® Titan Xp, NVIDIA GeForce® RTX 2080 Ti, NVIDIA Titan V, and NVIDIA GeForce GTX 1080.

The baseline method to assess the improvement achieved with the proposed method comprehend the usage of the WVR without the symmetric extension and, consequently, without the fixed stride crops. The WVR is resized to match the network input dimensions. All the network details described in the previous paragraph were also used in this baseline method. Table 5.1 shows the accuracy achieved by the baseline method with horizontal and vertical rhythms, WVR_y and WVR_x respectively.

Table 5.1: Baseline accuracy rates (%) for UCF101 and HMDB51.

Method	UCF101 (%)	HMDB51 (%)
WVR_y	65.19	34.46
WVR_x	60.41	32.37

The representation of the video through the WVR depends on the choice of two parameters: a reference row α_y or column α_x and the standard deviation σ_y or σ_x. The impacts of these parameters are explored in the first two experiments. The results show that the right choice of these parameters can help to improve the accuracy in both datasets. These results also provide evidence that the main action of the videos tends to focus on a particular region of the frames. We also perform experiments varying the symmetrical extension parameters aiming to achieve better settings for it. The results corroborate the assumption that a data augmentation method is essential for increasing the accuracy rates. The following sections discuss the experiments of the horizontal WVR and the vertical WVR separately, in this same order.

5.3 HORIZONTAL VISUAL RHYTHM PARAMETERIZATION

A sequence of experiments was performed to discover the best set of parameters for the SEVR$_y$. The baseline mean accuracy in this case is 65.19% and 34.46% in UCF101 and HMDB51 datasets (Table 5.1), respectively, and the baseline parameters were: $\alpha_y = 0.5$ and $\sigma_y = 33$. Throughout the experiments, the best parameters are employed in the subsequent executions. Initially, the parameters used for WVR and the symmetric extension are: $\alpha_y = 0.5$ (middle row), $n_c = 1$ and only the central crop in X is extracted. Since InceptionV3 expects input images of 299×299 pixels, w_{CNN} and h_{CNN} are both set to 299. The method depicted in Figure 4.2 was employed in all experiments.

In the first experiment, we compare the impact of the variation of the σ_y parameter. The following values for σ_y were tested: 7, 15, 33, 49 and 65. These values were chosen to verify if the region within the action occurs is concentrated in a small area or it is more vertically spread. According to the truncation of applied the Gaussian filter, the value 33 spans approximately 1/3 of the frame width. We empirically chose this value as the starting point for selecting the other valuers. The values smaller than 33 are approximately half and the 1/4 of the starting point, and the bigger ones are approximately the 50% increase and the double. The results are shown in Table 5.2. The better standard deviation for UCF101 was 33, and for HMDB51 it was 15. This indicates that actions on UFC101 tend to occur in a more spread region compared to HMDB51 since a smaller standard deviation means more concentrated Gaussian weighting around the middle row.

In the second experiment, we show the influence of the reference row on the accuracy

Table 5.2: Comparison of accuracy rates (%) for UCF101 and HDMB51 varying the σ_y parameter.

σ_y	UCF101 (%)	HMDB51 (%)
7	63.29	33.66
15	63.85	**33.99**
33	**65.26**	33.40
49	64.62	32.24
65	63.00	31.46

rate. As mentioned earlier, a factor α_y is used instead of the parameter y. We explore values close to the center of the video, expecting that the scene tends to be framed in the center of the video. The values chosen for the factor were: 0.40, 0.45, 0.50, 0.55 and 0.60. Values above 0.5 indicate the lower part of the image. Because the samples in both datasets come from multiple sources, the main action in each video may not happen exactly in the center of the video. This is the case of the UCF101. It was empirically observed that the better results were obtained when the reference row is located just below the center of the video. The mean action position in this dataset tends to be horizontally shifted around 5% below the center of the video (Table 5.3).

Table 5.3: Comparison of mean accuracy rates (%) of UCF101 and HMDB51 varying the α_y factor.

α_y	UCF101 (%)	HMDB51 (%)
0.40	62.82	30.06
0.45	64.83	31.00
0.50	65.26	**33.99**
0.55	**65.32**	33.35
0.60	65.24	33.48

In the next experiment, the number of crops n_c is increased to check if the accuracy rate also increases. The premise is that with more crops, it is possible to cover the entire temporal extension of the video present in SEVR. It is expected that the new crops incorporate more discriminant aspects of the video. As mentioned before, the additional crops also increase the probability to get at least one crop matching an entire cycle of action. The n_c values used are: 1, 2, 3 and 4. In this experiment, the stride s between the crops is fixed to 299 matching the w_{CNN} size. Thus, consecutive and non-overlapping crops are obtained. Table 5.4 shows the results of this experiment. The results endorse

the expected correlation between n_c and the accuracy rate. We could explore even bigger values for n_c. However, we chose not to perform experiments with larger values because of the time spent in the training, that was almost 2 days for all splits of UCF101 and HMDB51, using the Titan Xp graphics card and $n_c = 4$. For the next experiments, we set the number of crops to 4.

Table 5.4: Comparison of accuracy rates (%) of UCF101 and HMDB51 datasets varying n_c parameter.

n_c	UCF101 (%)	HMDB51 (%)
1	65.32	33.99
2	65.64	34.42
3	66.19	34.03
4	**67.70**	**34.99**

The fourth experiment consists of using crops that overlap each other along the time dimension. When the extended WVR completes a cycle, it begins to repeat its temporal patterns, as shown in Figure 4.5. In the even WVR copies, those patterns are horizontally flipped. Crops can be extracted along the extended time dimension with or without direct overlapping, consecutively or not. Consecutive and non-overlapping neighbor crops are obtained with $s = w_{CNN}$, as in the previous experiment. Gaps between the crops are obtained by using stride $s > w_{CNN}$. Overlaps between consecutive crops occur when using $s < w_{CNN}$. In the present work, we investigate the cases having $0 < s \leq w_{CNN}$. Notice that multiple parts of the WVR, forward or backward in time, will be repeated if

$$w_{CNN} + (n_c - 1) \cdot s > f \tag{5.1}$$

is satisfied. Previous to the training, the rhythm is extended according to the number of crops n_c and the stride s employed in the experiment. Hence, the video samples satisfying Equation 5.1 are extended. Among the UCF101 videos, this occurs to 93.75% using stride 13, 95.47% using stride 25, and to all videos except for one using strides 274, 286, and 299. Concerning the HMDB51 videos, this occurs to 98.32% using stride 13, 98.82% using stride 25, and occurs all videos using the other values of stride. Table 5.5 display this statistic.

We used the strides 13, 25, 274, 286 and 299. According to the frame rate, these values have a direct relation with the time in video . Since all videos have 25 fps, each 25 columns

Table 5.5: Percentage of samples that are extended according to the employed stride s, with $w_{CNN} = 299$ and $n_c = 4$.

s	UCF101 (%)	HMDB51 (%)
13	93.75	98.32
25	95.47	98.82
274	$\simeq$100.0	100.0
286	$\simeq$100.0	100.0
299	$\simeq$100.0	100.0

of the WVR represents one second of the video. With a stride of 25, for instance, two consecutive crops overlap each other along their entire length except for the first second of the current crop and the last second of the next crop. On the other hand, with a stride of 274, the overlap occurs only between the last second of a crop and the first second of the next crop. Table 5.6 shows the results of this experiment. Notice that $s = 299$ provided the best accuracy for both datasets. This is the same CNN input width, which mean no direct overlap between consecutive crops. Further experiments are necessary to check if there is some relation between the stride s and the architecture input size.

Table 5.6: Comparison of accuracy rates (%) for UCF101 and HMDB51 varying the stride s parameter.

s	UCF101 (%)	HMDB51 (%)
13	66.26	34.10
25	65.60	33.75
274	66.56	33.86
286	66.18	34.09
299	**67.70**	**34.99**

Notice, in Figure 4.5, that the VR pattern of the first and third copies are the same as well as the second and fourth copies. Thus, a crop which contemplates part of the first VR copy could present an indirect overlap with another crop composed of a piece of the third VR copy inside that SEVR, for instance. This means that even using a stride $s \geq w_{CNN}$ an overlap can occur between crops. Experiments exploring this indirect overlap are not the focus of this work but could be present in future research.

We also used the top and bottom regions in X direction. Therefore, each video is covered with 12 windows. The results are presented in Table 5.7, using the best parameters found in previous experiments: $n_c = 4$ and $s = 299$ for both datasets, $\alpha_y = 0.55$ and

$\sigma_y = 0.33$ for UCF101 and $\alpha_y = 0.5$ and $\sigma_y = 0.15$ for HMDB51. Its worth note that some videos from HMDB51 (around 6.03%) did not benefit from the extra crops or benefited very poorly due to their frame width being under of w_{CNN} or very close to it. Thus, the new crops did not add supplementary information about the video aspects. Still, the extra eight crops helped to increase the accuracy rate in both datasets. Similar to the previous experiment, the use of the other regions produced an overlap between the crops along the spatial dimension. However, more experiments need to be performed to assess how the overlap in X can be explored for data augmentation.

Table 5.7: Comparison of accuracy rates (%) for UCF101 and HMDB51 when extra crops are used.

Regions	UCF101 (%)	HMDB51 (%)
Central	67.70	34.99
Central + Top + Bottom	**68.01**	**35.29**

Figure 5.1 show for UFC101 and HMDB51 the mean accuracy difference between the best result of SEVR$_y$ (Table 5.7) and the baseline method WVR. Blue bars mean the SEVR$_y$ were better by the given amount. Conversely, red bars favor the WVR. For the UCF101, SEVR$_y$ performs better in 68 classes, worse in 32 classes, with even results in 1 classes. For the HMDB51, SEVR$_y$ performs better in 25 classes, worse in 23 classes, with even results in 3 classes. The classes which demonstrated improvement for the proposed method seem to share some characteristics among each other. They often present actions with certain cyclic movements (e.g., *brushing teeth, playing violin, typing*). This kind of action takes full advantage of the SEVR$_y$. Since the reverse movement generates patterns very similar to the one generated by the original movement, the multiple crops reinforce this kind of action and increase the accuracy of them, corroborating with our premise.

In UCF101, the top-5 actions where SEVR was inferior to WVR are *apply lipstick*, *drumming*, *handstand push ups*, *pull up* and *push up*, respectively indices 2, 27, 37, 70 and 72, and the top-5 actions where SEVR was superior to WVR are *biking*, *cutting in kitchen*, *mopping floor*, *playing dhol* and *tai chi*, respectively indices 11, 25, 55, 61 and 91. In HMDB51, the top 5 actions where SEVR was inferior to WVR are *dive*, *punch*, *ride horse*, *shoot gun* and *sit up*, respectively indices 8, 28, 32, 37 and 39, and the top 5 actions where SEVR was superior to WVR are *catch*, *drink*, *eat*, *handstand* and *laugh*, respectively indices 3, 11, 12, 17 and 24. On both datasets, some of the top-

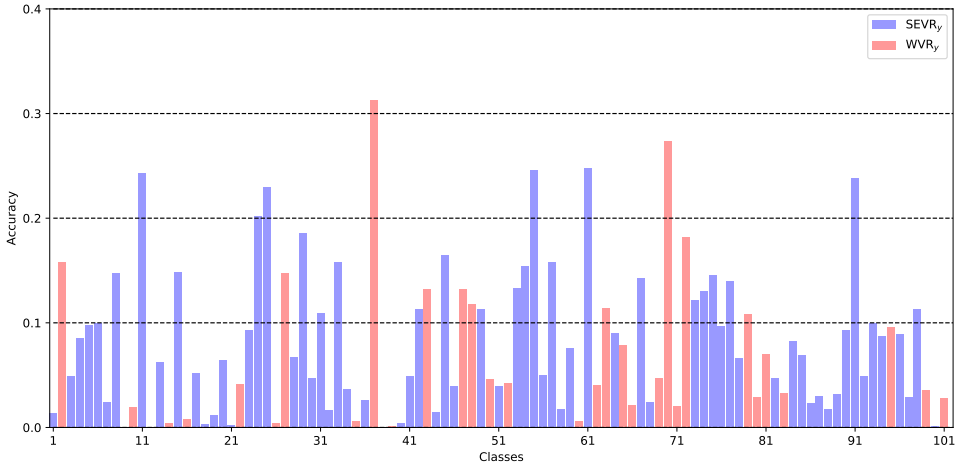

(a) UCF101

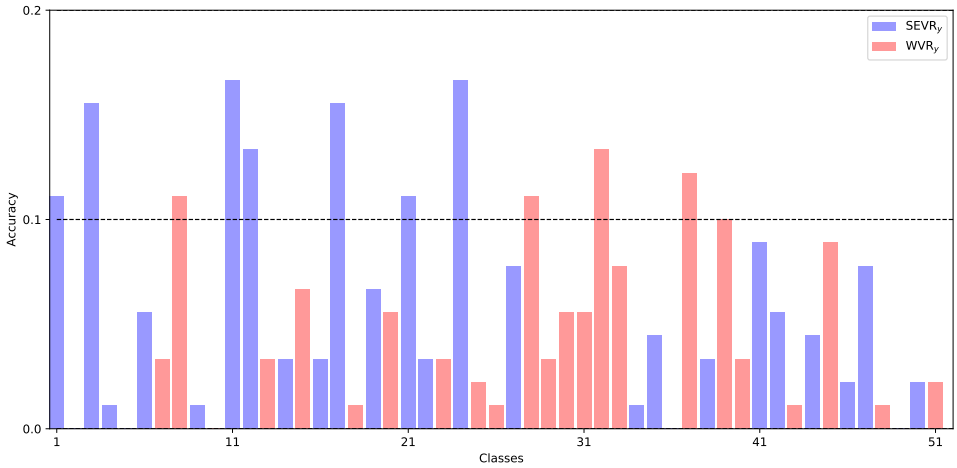

(b) HMDB51

Figure 5.1: Mean accuracy difference for each class between SEVR$_y$ and WVR$_y$ for UCF101 (a) and HMDB51 (b). Blue bars indicate that SEVR performs better by the given amount while red bars favor WVR.

5 actions that performed worst with SEVR in comparison with WVR are actions that could be treated as cyclic actions and thus exploited better the symmetric extension (e.g. *puch*, *pull up* and *push up*). Analogously, some actions that apparently do not show cyclic motion patterns and possibly be harmed by the symmetric extension are present in the top-5 actions where SEVR performed better than WVR (e.g. *tai chi*, *catch* and *handstand*). Despite that, the expected behavior of performance enhancement in cyclic actions can be observed from many of the top-5 actions where SEVR performed better than WVR, such as *biking*, *cutting in kitchen*, *mopping floor*, *playing dhol*, *drink* and *eat*. The aforementioned actions apparently do not have common aspects that indicate when the symmetric extension should be applied. Nevertheless, further investigation is necessary to understand the effects of employing the symmetric extension in some classes

and how this affect the signature patterns generated in the Visual Rhythms.

5.4 VERTICAL VISUAL RHYTHM PARAMETERIZATION

We repeated the same sequence of experiments to discover the best set of parameters for the SEVR$_x$. The baseline mean accuracy in this case is 60.41% and 32.37% in UCF101 and HMDB51 datasets (Table 5.1), respectively, and the baseline parameters were: $\alpha_x = 0.5$ and $\sigma_x = 33$. As in the previous section, the best parameter found in one experiment is also employed in the subsequent experiments. Initially, the parameters used for WVR and the symmetric extension are: $\alpha_x = 0.5$ (middle column), $n_c = 1$ and only the central crop in Y is extracted. Since InceptionV3 expects input images of 299×299 pixels, w_{CNN} and h_{CNN} are both set to 299. Considering that the videos of the UCF101 dataset have fixed dimensions of 320×240, the crops extracted from the vertical WVR are resized in spatial dimension to match the h_{CNN} dimension. The method depicted in Figure 4.2 was employed in all experiments.

The first experiment compares the impact of the variation of the σ_x parameter. The same values from the horizontal rhythm are used for σ_x: 7, 15, 33, 49 and 65. The results are shown in Table 5.8. The better standard deviation for UCF101 was again 33, and for HMDB51 was 65. It is worth noting that the standard deviation 33 for the vertical rhythm of the UCF101 indicates a more significant scattering if compared with its horizontal counterpart due to the mentioned size difference between frame dimensions. The result for HMDB51 indicates an even more spread motion pattern across the vertical axis in contrast to the value found in the same experiment for the horizontal rhythm of this dataset.

Table 5.8: Comparison of accuracy rates (%) for UCF101 and HDMB51 varying the σ_x parameter.

σ_x	UCF101 (%)	HMDB51 (%)
7	60.48	27.64
15	61.15	28.50
33	**62.22**	29.89
49	62.05	30.33
65	60.73	**31.39**

In the second experiment, we show the influence of the reference column on the ac-

curacy rate. As mentioned earlier, a factor α_x is used instead of the parameter x. The values from the corresponding experiment of the previous section repeat here: 0.40, 0.45, 0.50, 0.55 and 0.60. The results of Table 5.9 suggest that the middle column and its surrounding region are the areas with more occurrence of vertical motion. The best value for the α_x on both datasets was 0.50.

Table 5.9: Comparison of mean accuracy rates (%) of UCF101 and HMDB51 varying the α_x factor.

α_x	UCF101 (%)	HMDB51 (%)
0.40	58.14	31.31
0.45	61.06	31.09
0.50	**62.20**	**31.39**
0.55	61.47	30.83
0.60	58.42	29.10

In the next experiment, we check if the correlation between the number of windows n_c and accuracy rate holds for the vertical WVR. The premise is the same as the horizontal rhythm. It is expected that the new crops incorporate more discriminant aspects of the video and increase the chance of at least one of them contains an entire cycle of action. The n_c values used are: 1, 2, 3 and 4. The stride s between the windows is fixed to 299 matching the w_{CNN} size. Thus, consecutive and non-overlapping crops are obtained. Table 5.10 show the results of this experiment. Despite some decrease with 3 crops in the UCF101 and 2 crops in the HMDB51, in the long term, the correlation between n_c and the accuracy rate is showed.

Table 5.10: Comparison of accuracy rates (%) of UCF101 and HMDB51 datasets varying n_c parameter.

n_c	UCF101 (%)	HMDB51 (%)
1	62.20	31.39
2	62.59	29.8
3	61.75	31.72
4	**63.50**	**32.11**

The fourth experiment evaluates the stride value s. The same statements about the stride variation mentioned in the corresponding experiment of the previous section also concern to the vertical rhythm. The same stride were used: 13, 25, 274, 286 and 299.

Table 5.11 shows the results of this experiment. The same results of the horizontal rhythm have repeated for the vertical one.

Table 5.11: Comparison of accuracy rates (%) for UCF101 and HMDB51 varying the stride s parameter.

s	UCF101 (%)	HMDB51 (%)
13	62.09	30.22
25	61.90	31.81
274	62.31	30.68
286	62.73	30.15
299	**63.50**	**32.11**

The final experiment consisted in the usage of top and bottom regions in Y direction. However, since the height h of the videos of the UCF101 dataset is smaller than the h_{CNN}, there is not a reminiscent region to be covered. All the spatial dimension data is represented in the vertical WVR. Despite this, for completeness of the experiments and to evaluate the impact of the replication of the exact information contained in one crop, we have used the same n_c crops three times, one for each region (center, top, and bottom). Therefore, in this experiment, each video was covered by 12 windows using the best parameters found in the previous experiments for each dataset. The results are presented in Table 5.12. The impact of the replication is negative for the two datasets. Consequently, the usage of 4 distinct crops from the vertical rhythm is better than 12 crops with repeated information.

Table 5.12: Comparison of accuracy rates (%) for UCF101 and HMDB51 when extra crops are used.

Regions	UCF101 (%)	HMDB51 (%)
Central	**63.50**	**32.11**
Central + Top + Bottom	62.81	30.85

Figure 5.2 shows for UFC101 and HMDB51 the mean accuracy difference between the best result of SEVR$_x$ (Table 5.12) and the baseline method WVR. Blue bars mean the SEVR$_x$ were better by the given amount. Conversely, red bars favor the WVR. For the UCF101, SEVR$_x$ performs better in 55 classes, worse in 45 classes, with even results in 1 classes. For the HMDB51, SEVR$_x$ performs better in 23 classes, worse in 26 classes, with even results in 2 classes.

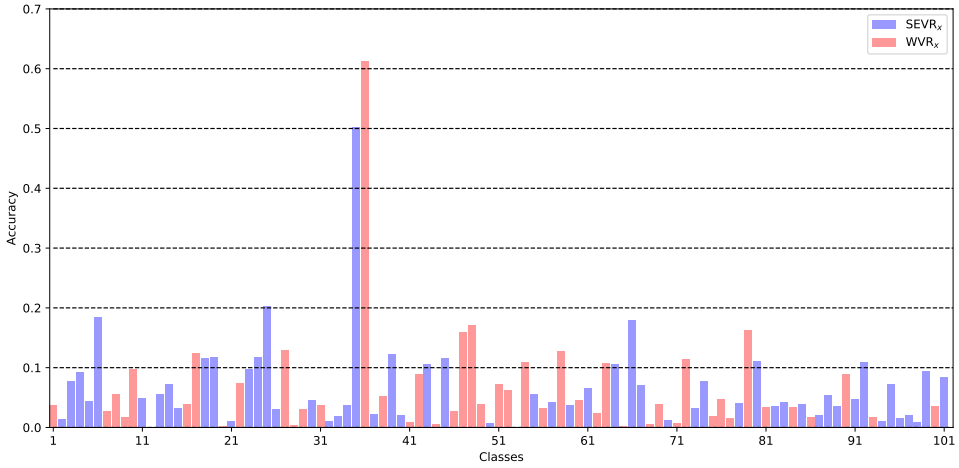

(a) UCF101

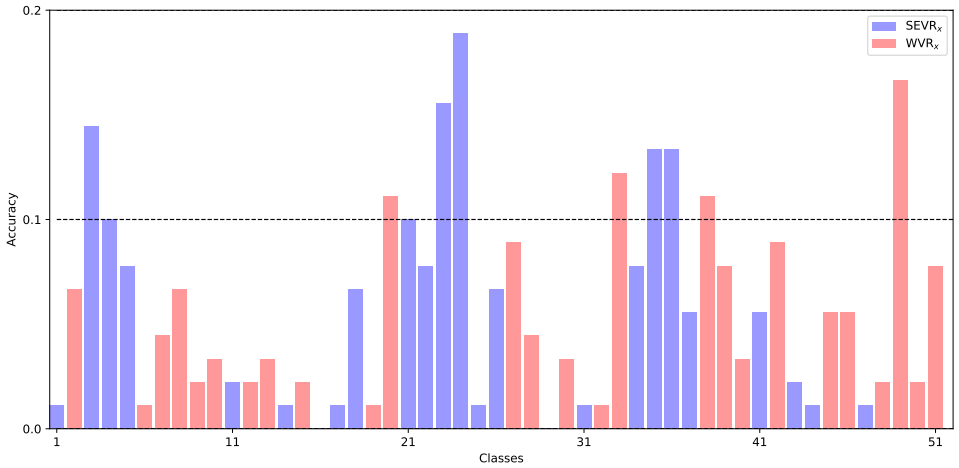

(b) HMDB51

Figure 5.2: Mean accuracy difference for each class between SEVR$_x$ and WVR$_x$ for UCF101 (a) and HMDB51 (b). Blue bars indicate that SEVR performs better by the given amount while red bars favor WVR.

In UCF101, the top 5 actions where SEVR was inferior to WVR are *drumming*, *hammer throw*, *jumping jack*, *jump rope* and *shot put*, respectively indices 27, 36, 47, 48 and 79, and the top 5 actions where SEVR was superior to WVR are *band marching*, *cutting in kitchen*, *hammering*, *head massage* and *playing tabla*, respectively indices 6, 25, 35, 39 and 66. In HMDB51, the top 5 actions where SEVR was inferior to WVR are *jump*, *run*, *sit*, *somersault* and *turn*, respectively indices 20, 33, 38, 42 and 49, and the top 5 actions where SEVR was superior to WVR are *catch*, *kiss*, *laugh*, *shoot ball* and *shoot bow*, respectively indices 3, 23, 24, 35 and 36. As noted for the horizontal rhythm, the results mix some expected and unexpected behaviors. It is worth mentioning that some classes that were among the top-5 enhanced classes with SEVR$_y$ also belong to the same group concerning to SEVR$_x$: *cutting in kitchen* from UCF101, and *catch* and *laugh* from

HMDB51. This reinforces the importance of SEVR to increase these classes accuracies.

5.5 DATA AUGMENTATION ABLATION STUDY

In this section, we present an experiment to evaluate the real contribution of our data augmentation method apart from Keras data augmentation methods. To this end, we executed the baseline method without Keras data augmentation (horizontal flip, vertical flip, and zoom in the range of 0.8 to 1.2). The baseline method does not count with our proposed data augmentation with fixed stride crops taken from the symmetric extension. Therefore, this is the scenario without any other data augmentation methods. We already have the results of the previous sections that take advantage of both data augmentation methods (Keras and ours). To complete the experiment setup, we already run the scenario with our data augmentation and without Keras' data augmentation. Table 5.13 show the results of these experiments. All results were obtained using the horizontal version of the WVR. The SEVR scenarios used 4 crops with fixed stride of 299.

Table 5.13: Comparison of accuracy rates (%) for UCF101 and HMDB51 with (w/) and without (w/o) data augmentation methods.

Scenarios	UCF101 (%)		HMDB51 (%)	
	w/ Keras DA	w/o Keras DA	w/ Keras DA	w/o Keras DA
Baseline	65.19	57.64	34.46	28.93
SEVR	67.70	60.55	34.99	28.80

In both datasets, we can notice that the conventional data augmentation methods performed for image classification are also applicable for VRs. The results are very significant with a mean difference of 7.35% and 5.86%, in UCF101 and HMDB51 respectively, in favor of the usage of Keras data augmentation. The performance increase with our data augmentation methods on UCF101 was very relevant too. In this dataset, the mean increase was 2.71%. However, for HMDB51, our approach showed a slight decrease without using Keras data augmentation, 0.13%, and a small increase using both data augmentation methods, 0.53%. In future works, we intend to investigate better the behavior of data augmentation methods on HMDB51. Overall, the usage of both data augmentation methods for both datasets leads to the performance increase, highlighting the performance in UCF101, which increased over 10%.

5.6 MULTI-STREAM CLASSIFICATION USING VISUAL RHYTHMS

The goal in this section is to show that our spatiotemporal streams can complement a multi-stream architecture to get more competitive accuracy rates. The results of individual streams are shown in Table 5.14. The first five approaches, Optical Flow, RGB*, Horizontal-mean, Vertical-mean, and Adaptive Visual Rhythm (AVR), are results from the work of Concha et al. (2018). It is worth remembering that the use of OF as a temporal stream is not a contribution of Concha et al. (2018), but of Simonyan and Zisserman (2014a). However, the result of such work is shown since it comes from the use of the InceptionV3 network in the temporal stream, which is not performed in the original two-stream work (SIMONYAN; ZISSERMAN, 2014a). Similar to other multi-stream networks (SIMONYAN; ZISSERMAN, 2014a; WANG et al., 2015b), the OF performs better in both datasets. It is possible to notice that the horizontal SEVR presented superior performance if compared with the vertical one, independent of the dataset. The same outcome appeared in the mean rhythm results. Excepting for the SEVR_y in the HMDB51, the SEVR was superior to the mean rhythm approach. Concerning the comparison between the SEVR_y with the AVR, the results are divided. Even using only horizontal motion information, the SEVR_y is better than AVR in the UCF101 scenario. However, the lack of vertical information may be one of the factors that led to a worse result in the HMDB51 dataset.

Table 5.14: Results of single-stream approaches.

Single streams	UCF101 (%)	HMDB51 (%)
Optical Flow (CONCHA et al., 2018)	**86.95**	**59.91**
RGB* images (CONCHA et al., 2018)	86.61	51.77
Horizontal - mean (CONCHA et al., 2018)	62.37	35.57
Vertical - mean (CONCHA et al., 2018)	53.87	30.12
AVR (CONCHA et al., 2018)	64.74	39.63
WVR_y	65.19	34.46
WVR_x	60.41	32.37
SEVR_y	68.01	35.29
SEVR_x	63.50	32.11

In order to our approach achieve more competitive results, we proposed a final multi-stream architecture merging the SEVR_y and SEVR_x best setups, with the RGB* and the OF streams. This final combination is not enough to assess the complementarity of the

streams. To this end, we also conducted experiments incrementally fusing the streams.

The strategy used for merging the streams was the same described by Concha et al. (2018). More specifically, to fuse the predictions of all streams, weights were evaluated through a grid search strategy. For each weight, we tested every value from 0 to 10 with a 0.5 step. We are aware that this is not the best strategy for merging the streams. However, its adoption allows an impartial attribution of weights and proper comparison between the results of Concha et al. (2018) with the results of the present work. Besides, the proposition of a new approach for late fusion is not the focus of the present work. This is an open question that could be the focus of future works. Concerning the combination of all streams, the best combination found for UCF101 was 9.0, 7.0, 1.5 and 1.5, respectively for OF, RGB*, SEVR_y and SEVR_x. And the best combination found for HMDB51 was 7.5, 3.5, 1.0 and 0.5, respectively for OF, RGB*, SEVR_y and SEVR_x. We obtained 93.94% for UCF101 and 67.73% for HMDB51. It was observed that higher accuracy is reached when the combination is done with the feature maps before the softmax normalization, as well as performed in the classification with multiple fixed stride crops.

Table 5.15 shows the results of the incremental experiments. It contains the $\binom{4}{2}$ combinations, $\binom{4}{3}$ combinations and the combination of all streams. In these results, it is possible to observe a standard behavior. The combination of the best single-streams (OF and RGB*) generated the best two-stream combination, and the merging of the best two-stream formed the best three-stream combination with the third best single-stream result (SEVR_y). However, there is no guarantee that the best results are also the most complementary among each other. This is verified, in the UCF101 scenario, by the best two-streams containing SEVR_y and SEVR_x separately, which are formed with RGB* instead of OF. So, the other streams are crucial to complement the OF and to improve accuracy when combined.

Table 5.15 also shows the simple sum for the best combinations in each modality. In this case, we used the feature maps after the softmax normalization because of the magnitude difference between streams. The simple sum is the merge strategy adopted by some works on literature (SIMONYAN; ZISSERMAN, 2014a; WANG et al., 2015b). Although the impact on two-stream is not harmful, the results tend to be more negatively affected by the streams increase, which is possibly a consequence of the accuracy gap among the streams. The superior results of the weighted sum in all cases demonstrate

Table 5.15: Results of the combination of the streams.

Streams	UCF101 (%)	HMDB51 (%)
OF + RGB*	**93.21**	**66.43**
OF + $SEVR_y$	89.07	62.85
OF + $SEVR_x$	88.50	61.68
RGB* + $SEVR_y$	89.87	56.49
RGB* + $SEVR_x$	88.83	55.75
$SEVR_y$ + $SEVR_x$	75.90	41.85
OF + RGB* + $SEVR_y$	**93.70**	**67.15**
OF + RGB* + $SEVR_x$	93.53	66.91
OF + $SEVR_y$ + $SEVR_x$	89.72	63.20
RGB* + $SEVR_y$ + $SEVR_x$	90.76	58.43
All streams	**94.06**	**67.73**
Simple mean of OF + RGB*	**92.06**	**65.03**
Simple mean of OF + RGB* + $SEVR_y$	91.01	60.98
Simple mean of all streams	90.17	58.45

that the methods that treat each stream differently lead to better results in multi-stream architectures.

Furthermore, the two-stream combination of our both spatiotemporal stream ($SEVR_y$ + $SEVR_x$ line on Table 5.15) surpassed the AVR (Table 5.14). Both methods combined data about horizontal and vertical motion. While this comparison is not fair, because the two-stream had two types of data per sample and the AVR counts with only one type per sample, it gives a clue that combining vertical and horizontal motion is more advantageous than using the information from the most prominent movement direction.

Table 5.16 presents a comparison of our method combining all stream features through multi-stream late fusion and the other methods in the literature. In this table, there are also some pioneer works on the field. Our multi-stream approach was based on these works, and our method was able to improve their performance. Although the $SEVR_y$ and $SEVR_x$ streams do not achieve accuracy rates comparable to the SOTA individually (Table 5.16), the improved multi-stream method produced fairly competitive accuracy rates.

However, our method is overcome by some works. The works pre-trained with the Kinetics (KAY et al., 2017) dataset have access to a volume of information that is crucial to achieving higher accuracy on UCF101 and HMDB51. However, a substantial amount

Table 5.16: Comparison of accuracy rates (%) for UCF101 and HMDB51 datasets.

Method	Pre-training Dataset	UCF101 (%)	HMDB51 (%)
Two-Stream I3D (CARREIRA; ZISSERMAN, 2017)	ImageNet + Kinetics	98.0	80.7
I3D + PoTion (CHOUTAS et al., 2018)	ImageNet + Kinetics	**98.2**	80.9
SVMP+I3D (WANG et al., 2018)	ImageNet + Kinetics	—	81.3
DTPP (ZHU et al., 2018)	ImageNet + Kinetics	98.0	**82.1**
TDD+IDT (WANG et al., 2015a)	ImageNet	91.5	65.9
TVNets+IDT (FAN et al., 2018)	ImageNet	**95.4**	**72.6**
OFF (SUN et al., 2018)	—	**96.0**	**74.2**
Two-Stream (SIMONYAN; ZISSERMAN, 2014a)	ImageNet	88.0	59.4
Two-Stream TSN (WANG et al., 2016a)	ImageNet	94.0	68.5
Three-Stream TSN (WANG et al., 2016a)	ImageNet	94.2	69.4
Three-Stream (WANG et al., 2017)	ImageNet	94.1	70.4
KVMDF (ZHU et al., 2016)	ImageNet	93.1	63.3
STP (WANG et al., 2017a)	ImageNet	94.6	68.9
Multi-Stream + ResNet152 (CONCHA et al., 2018)	ImageNet	94.3	68.3
Multi-Stream + InceptionV3 (CONCHA et al., 2018)	ImageNet	93.7	69.9
Our method	ImageNet	94.1	67.7

of computational power required for pre-training with Kinetics makes its use impractical in most cases. Thus, we do not consider a direct comparison with these approaches. The merging with IDT features (WANG; SCHMID, 2013) is another way to increase performance. DL methods often benefit from exploring this specific hand-crafted feature. In future works, we plan to verify the complementarity of this feature with our SEVR. Furthermore, the OFF approach stands out by being a method that does not use Kinectics pre-training and still achieves very close results to those that explores it. The presented result is a combination of a RGB and a OF streams with the OFF method applied to RGB, OF, and RGB difference, also exploring the complementarity of some different features.

Considering the UCF101 and VR approaches, our method outperforms the proposal of Concha et al. (2018), using the InceptionV3. Our approach is not better than the ResNet152 result for the UCF101. The ResNet152 is deeper than the InceptionV3, and this may be the reason for the difference between outcomes. Considering that our approach used four streams, the change to a deeper model certainly would increase significantly the computational time required for training and testing. Further investigation is needed to evaluate the deep-accuracy trade-off on multi-stream architectures. While compared to the results of Concha et al. (2018), our SEVR method did not show a performance improvement as good in HMDB51 as in UCF101 dataset. We conjectured that this difference might be due to the high level of video resolution heterogeneity among samples present in

HMDB51 together with the usage of fixed parameters to all samples. Thus, this dataset may benefit best from adaptive methods, such as the AVR approach.

The confusion matrices of our multi-stream method applied for UCF101 and HMDB51, respectively, are shown in Figures 5.3 and 5.4. The numeric indexes are according to the alphabetical order of the classes. On UCF101 is possible to notice a reasonable misclassification between *body weight squats* and *lunges* classes (indices 15 and 52 respectively) because their similar motion aspect. On HMDB51, a misclassification occurs between *sit* and *stand* classes (indices 38 and 43 respectively) which is probably due to the usage of the SEVR since, in this specific situation, time direction is crucial to distinguish the actions.

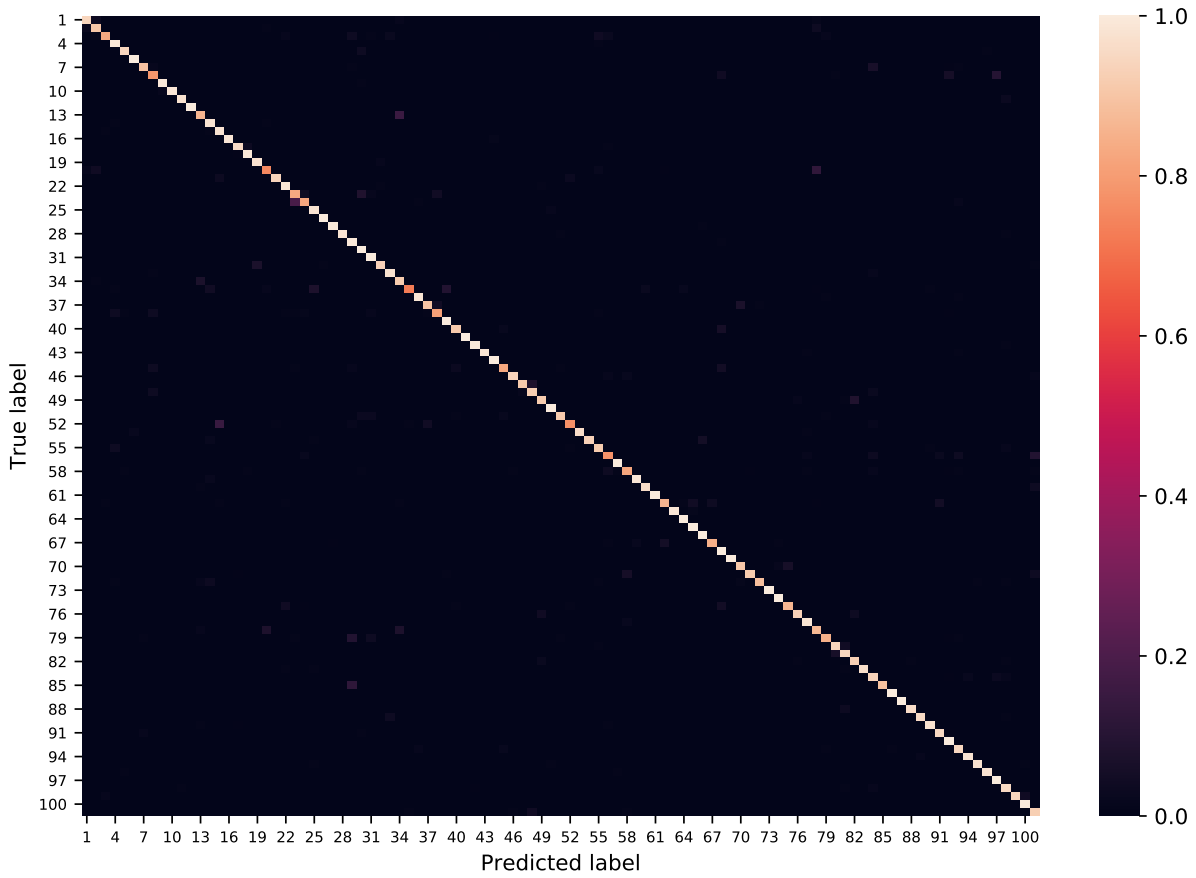

Figure 5.3: Mean confusion matrix of the final multi-stream method for UCF101.

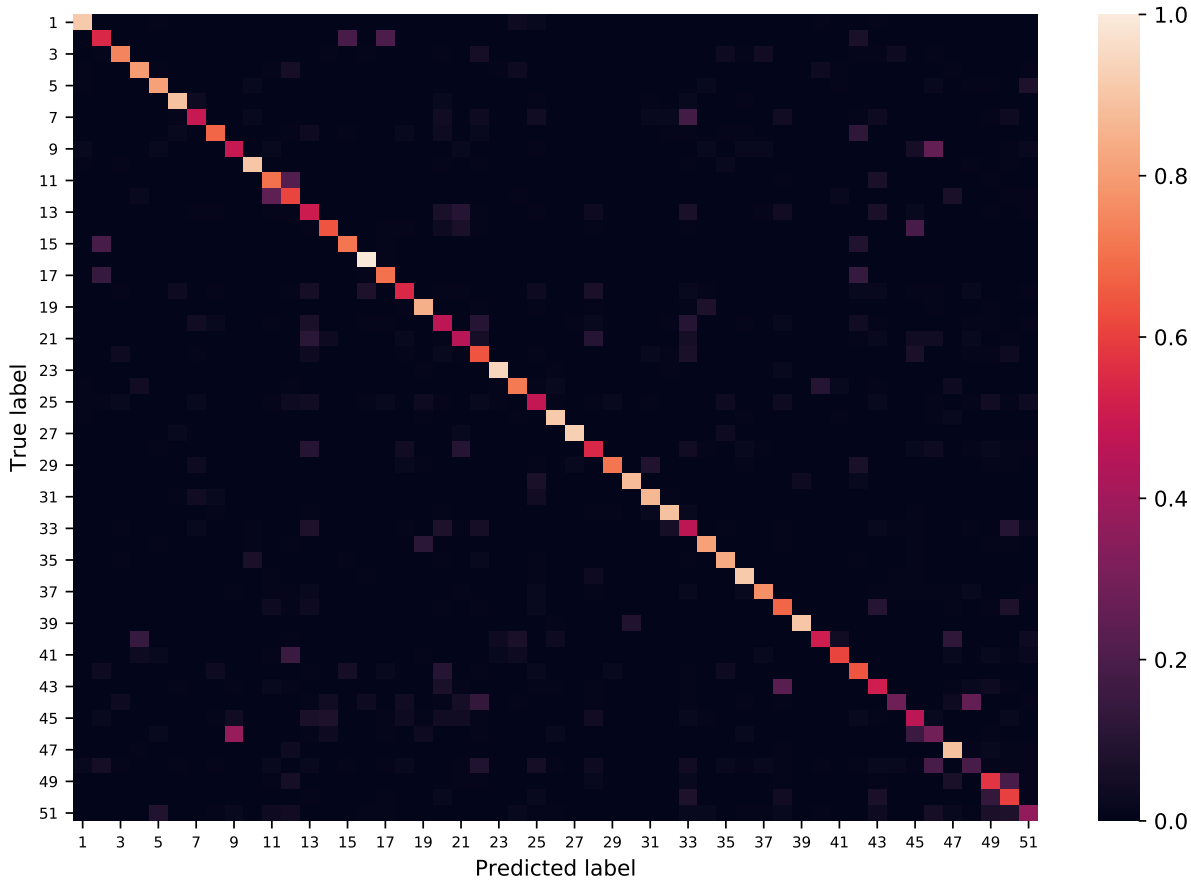

Figure 5.4: Mean confusion matrix of the final multi-stream method for HMDB51.

6 CONCLUSIONS AND FUTURE WORK

In this present work, we propose an approach to deal with HAR in videos. It consists of the improvement of a two-stream method reasoned on the inclusion of complementary information through two spatiotemporal streams. The proposed spatiotemporal streams are 2D CNNs operating on a new VR named WVR. The WVR was based on the premise that the motion on videos tends to concentrate in particular areas. The VR, in general, is a method that applies an extreme pooling in the spatial data and keeps all temporal information of this pooled data. This drives to a problem related to its temporal dimension and the usage of CNNs that have a fixed input size. The VR's temporal dimension is restricted to the video length, and the rescale of this dimension requires some caution. Any transformation in this dimension would interfere in the video sample rate. To circumvent this problem, we propose to extend the VR symmetrically in time.

We observed that the direction of video execution does not discriminate aspects of various actions. Thus, the inverse action could be recognized as well as the action being performed in its normal course. Based on this premise, we propose the SEVR. The SEVR consists of concatenating several VR copies along the time dimension with the even repetitions horizontally flipped. This is equivalent to replicate periodically the frames backward in time when the video reaches its end, and then replicate the frames normally when it reaches the beginning again. Thus, it is possible to extract as many as required crops, apart from each other by a stride, from the SEVR with any demanded temporal size. The SEVR maintains the video frame rate and allows multiple samples of the underlying motion pattern to be obtained. It also provides data augmentation, which is valuable for training 2D CNNs with small datasets.

Furthermore, we evaluate these methods through the exploration of its parameters and the combination of the OF and RGB streams with two spatiotemporal streams, each one operating in one distinct SEVR (horizontal and vertical). Experimental results show that SEVR improves accuracy rates if compared to the resized WVR, indicating that the symmetric extension is helpful to bypass the temporal constraints of video samples. In future works, the SEVR principles could also be employed to 3D CNNs for video classification problems. For HMDB51, the improvement showed by the results was less significant.

We conjectured that this might be due to the high level of video resolution heterogeneity among samples present in HMDB51 together with the usage of fixed parameters to all samples. We intend to tackle this problem in future works by using adaptive parameters at the sample level for the WVR extraction. The assumption is that among the HMDB51 samples, there is a considerable variation in the positioning of the action inside the frame. Thus, a position estimation of the region with more motion for each sample might create a WVR that represents better the motion behind the video. We also evaluated the influence of the conventional data augmentation for image classification in the VRs. It was verified that these data augmentation methods are very relevant for HAR using VRs and that the data augmentation provided by the SEVR with fixed stride crops is also appropriate independently of the usage of those other augmentation methods.

Concerning our multi-stream architecture, the results endorsed the complementarity between the spatial and temporal streams with our spatiotemporal streams. Our approach did not surpass some state-of-the-art methods, but it was able to assess the improvement that multi-stream architecture could benefit from spatiotemporal streams. To achieve more competitive results, in future works, we pretend to explore the complementarity of our multi-stream architecture with other features, such as IDT (WANG et al., 2013) and I3D (CARREIRA; ZISSERMAN, 2017). Other proposals for future works are listed below:

- Explore the SEVR on larger datasets, e.g., Kinetics (KAY et al., 2017), YouTube-8M (ABU-EL-HAIJA et al., 2016);
- Explore different stream fusion approaches, e.g., class-level fusion, sample-level fusion;
- Explore different crop sizes and random crop positioning for SEVR;
- Evaluate the trade-off between deeper architectures and accuracy for multi-stream training;
- Investigate and elaborate a specific DL architecture to use VRs as inputs.

REFERENCES

ABU-EL-HAIJA, S.; KOTHARI, N.; LEE, J.; NATSEV, P.; TODERICI, G.; VARADARAJAN, B.; VIJAYANARASIMHAN, S. Youtube-8M: A large-scale video classification benchmark. **arXiv preprint arXiv:1609.08675**, 2016.

ASLANI, S.; MAHDAVI-NASAB, H. Optical flow based moving object detection and tracking for traffic surveillance. **International Journal of Electrical, Computer, Energetic, Electronic and Communication Engineering**, v. 7, n. 9, p. 1252–1256, 2013.

BALLAS, N.; YAO, L.; PAL, C.; COURVILLE, A. Delving deeper into convolutional networks for learning video representations. **arXiv preprint arXiv:1511.06432**, 2015.

BAY, H.; TUYTELAARS, T.; GOOL, L. V. Surf: Speeded up robust features. In: SPRINGER. **European Conference on Computer Vision**, 2006. p. 404–417.

BIAN, Y.; GAN, C.; LIU, X.; LI, F.; LONG, X.; LI, Y.; QI, H.; ZHOU, J.; WEN, S.; LIN, Y. Revisiting the effectiveness of off-the-shelf temporal modeling approaches for large-scale video classification. **arXiv preprint arXiv:1708.03805**, 2017.

BILEN, H.; FERNANDO, B.; GAVVES, E.; VEDALDI, A.; GOULD, S. Dynamic image networks for action recognition. In: **IEEE Conference on Computer Vision and Pattern Recognition**, 2016. p. 3034–3042.

BLANK, M.; GORELICK, L.; SHECHTMAN, E.; IRANI, M.; BASRI, R. Actions as Space-Time Shapes. In: **International Conference on Computer Vision**, 2005. p. 1395–1402.

BROX, T.; BRUHN, A.; PAPENBERG, N.; WEICKERT, J. High accuracy optical flow estimation based on a theory for warping. In: SPRINGER. **European Conference on Computer Vision**, 2004. p. 25–36.

CANZIANI, A.; PASZKE, A.; CULURCIELLO, E. An analysis of deep neural network models for practical applications. **arXiv preprint arXiv:1605.07678**, 2016.

CARREIRA, J.; ZISSERMAN, A. Quo Vadis, Action Recognition? A New Model and the Kinetics Dataset. In: **IEEE Conference on Computer Vision and Pattern Recognition**, 2017. p. 4724–4733.

CHAARAOUI, A. A.; CLIMENT-PÉREZ, P.; FLÓREZ-REVUELTA, F. A review on vision techniques applied to human behaviour analysis for ambient-assisted living. **Expert Systems with Applications**, Elsevier, v. 39, n. 12, p. 10873–10888, 2012.

CHATFIELD, K.; SIMONYAN, K.; VEDALDI, A.; ZISSERMAN, A. Return of the Devil in the Details: Delving Deep into Convolutional Nets. **arXiv preprint arXiv:1405.3531**, 2014.

CHO, K.; MERRIËNBOER, B. V.; GULCEHRE, C.; BAHDANAU, D.; BOUGARES, F.; SCHWENK, H.; BENGIO, Y. Learning phrase representations using rnn encoder-decoder for statistical machine translation. **arXiv preprint arXiv:1406.1078**, 2014.

CHOLLET, F. Xception: Deep learning with depthwise separable convolutions. In: **Proceedings of the IEEE Conference on Computer Vision and Pattern Recognition**, 2017. p. 1251–1258.

CHOLLET, F. et al. **Keras**. 2015. `https://keras.io`.

CHOUTAS, V.; WEINZAEPFEL, P.; REVAUD, J.; SCHMID, C. Potion: Pose motion representation for action recognition. In: **IEEE Conference on Computer Vision and Pattern Recognition**, 2018.

CIPTADI, A.; GOODWIN, M. S.; REHG, J. M. Movement pattern histogram for action recognition and retrieval. In: SPRINGER. **European Conference on Computer Vision**, 2014. p. 695–710.

CONCHA, D. T.; MAIA, H. D. A.; PEDRINI, H.; TACON, H.; BRITO, A. D. S.; CHAVES, H. D. L.; VIEIRA, M. B. Multi-stream convolutional neural networks for action recognition in video sequences based on adaptive visual rhythms. In: **IEEE International Conference on Machine Learning and Applications**, 2018. p. 473 – 480. Disponível em: <https://doi.org/10.1109/icmla.2018.00077>.

DALAL, N.; TRIGGS, B. Histograms of oriented gradients for human detection. In: **International Conference on Computer Vision and Pattern Recognition**, 2005. v. 1, p. 886–893.

DALAL, N.; TRIGGS, B.; SCHMID, C. Human detection using oriented histograms of flow and appearance. In: SPRINGER. **European Conference on Computer Vision**, 2006. p. 428–441.

DENG, J.; DONG, W.; SOCHER, R.; LI, L.-J.; LI, K.; FEI-FEI, L. ImageNet: A Large-Scale Hierarchical Image Database. In: **IEEE Conference on Computer Vision and Pattern Recognition**, 2009.

DIBA, A.; SHARMA, V.; GOOL, L. V. Deep temporal linear encoding networks. In: **Proceedings of the IEEE Conference on Computer Vision and Pattern Recognition**, 2017. p. 2329–2338.

DONAHUE, J.; JIA, Y.; VINYALS, O.; HOFFMAN, J.; ZHANG, N.; TZENG, E.; DARRELL, T. Decaf: A deep convolutional activation feature for generic visual recognition. In: **International Conference on Machine Learning**, 2014. p. 647–655.

FAN, L.; HUANG, W.; GAN, C.; ERMON, S.; GONG, B.; HUANG, J. End-to-end learning of motion representation for video understanding. In: **Proceedings of the IEEE Conference on Computer Vision and Pattern Recognition**, 2018. p. 6016–6025.

FAWZI, A.; SAMULOWITZ, H.; TURAGA, D.; FROSSARD, P. Adaptive data augmentation for image classification. In: **2016 IEEE International Conference on Image Processing**, 2016. p. 3688–3692.

FEICHTENHOFER, C.; PINZ, A.; WILDES, R. Spatiotemporal residual networks for video action recognition. In: **Advances in Neural Information Processing Systems**, 2016. p. 3468–3476.

FEICHTENHOFER, C.; PINZ, A.; WILDES, R. P. Spatiotemporal multiplier networks for video action recognition. In: **IEEE Conference on Computer Vision and Pattern Recognition**, 2017. p. 7445–7454.

FEICHTENHOFER, C.; PINZ, A.; ZISSERMAN, A. Convolutional two-stream network fusion for video action recognition. In: **Proceedings of the IEEE Conference on Computer Vision and Pattern Recognition**, 2016. p. 1933–1941.

FERNANDO, B.; GAVVES, E.; ORAMAS, J. M.; GHODRATI, A.; TUYTELAARS, T. Modeling video evolution for action recognition. In: **Proceedings of the IEEE Conference on Computer Vision and Pattern Recognition**, 2015. p. 5378–5387.

GAO, Y.; BEIJBOM, O.; ZHANG, N.; DARRELL, T. Compact bilinear pooling. In: **Proceedings of the IEEE Conference on Computer Vision and Pattern Recognition**, 2016. p. 317–326.

GONZALEZ, R. C.; WINTZ, P. **Digital Image Processing (2nd Ed.)**, 1987. ISBN 0-201-11026-1.

GU, J.; WANG, Z.; KUEN, J.; MA, L.; SHAHROUDY, A.; SHUAI, B.; LIU, T.; WANG, X.; WANG, G. Recent Advances in Convolutional Neural Networks. **arXiv preprint arXiv:1512.07108**, 2015.

HE, K.; ZHANG, X.; REN, S.; SUN, J. Deep Residual Learning for Image Recognition. In: **IEEE Conference on Computer Vision and Pattern Recognition**, 2016. p. 770–778.

HORN, B. K.; SCHUNCK, B. G. Determining Optical Flow. **Artificial intelligence**, Elsevier, v. 17, n. 1-3, p. 185–203, 1981.

IOFFE, S.; SZEGEDY, C. Batch normalization: Accelerating deep network training by reducing internal covariate shift. **arXiv preprint arXiv:1502.03167**, 2015.

JI, S.; XU, W.; YANG, M.; YU, K. 3D Convolutional Neural Networks for Human Action Recognition. **IEEE Transactions on Pattern Analysis and Machine Intelligence**, IEEE, v. 35, n. 1, p. 221–231, 2013.

KARPATHY, A.; TODERICI, G.; SHETTY, S.; LEUNG, T.; SUKTHANKAR, R.; FEI-FEI, L. Large-Scale Video Classification with Convolutional Neural Networks. In: **IEEE Conference on Computer Vision and Pattern Recognition**, 2014. p. 1725–1732.

KAY, W.; CARREIRA, J.; SIMONYAN, K.; ZHANG, B.; HILLIER, C.; VIJAYANARASIMHAN, S.; VIOLA, F.; GREEN, T.; BACK, T.; NATSEV, P.; SULEYMAN, M.; ZISSERMAN, A. The Kinetics Human Action Video Dataset. **arXiv preprint arXiv:1705.06950**, 2017.

KIM, H.; LEE, J.; YANG, J.-H.; SULL, S.; KIM, W. M.; SONG, S. M.-H. Visual rhythm and shot verification. **Multimedia Tools and Applications**, Springer, v. 15, n. 3, p. 227–245, 2001.

KLASER, A.; MARSZAŁEK, M.; SCHMID, C. A spatio-temporal descriptor based on 3d-gradients. In: BRITISH MACHINE VISION ASSOCIATION. **BMVC 2008-19th British Machine Vision Conference**, 2008. p. 275–1.

KONG, Y.; FU, Y. Human action recognition and prediction: A survey. **arXiv preprint arXiv:1806.11230**, 2018.

KRIZHEVSKY, A.; SUTSKEVER, I.; HINTON, G. E. Imagenet Classification with Deep Convolutional Neural Networks. In: **Advances in Neural Information Processing Systems**, 2012. p. 1097–1105.

KUEHNE, H.; JHUANG, H.; STIEFELHAGEN, R.; SERRE, T. HMDB51: A Large Video Database for Human Motion Recognition. In: **High Performance Computing in Science and Engineering**, 2013. p. 571–582.

LAN, Z.; LIN, M.; LI, X.; HAUPTMANN, A. G.; RAJ, B. Beyond gaussian pyramid: Multi-skip feature stacking for action recognition. In: **Proceedings of the IEEE Conference on Computer Vision and Pattern Recognition**, 2015. p. 204–212.

LAPTEV, I.; MARSZALEK, M.; SCHMID, C.; ROZENFELD, B. Learning realistic human actions from movies. IEEE, 2008.

LIU, S.; YUAN, L.; TAN, P.; SUN, J. Steadyflow: Spatially smooth optical flow for video stabilization. In: **Proceedings of the IEEE Conference on Computer Vision and Pattern Recognition**, 2014. p. 4209–4216.

LIU, Z.; ZHANG, C.; TIAN, Y. 3d-based deep convolutional neural network for action recognition with depth sequences. **Image and Vision Computing**, Elsevier, v. 55, p. 93–100, 2016.

LOWE, D. G. Object recognition from local scale-invariant features. In: **Proceedings of the International Conference on Computer Vision-Volume 2 - Volume 2**, 1999. (ICCV '99), p. 1150–. ISBN 0-7695-0164-8. Disponível em: <http://dl.acm.org/citation.cfm?id=850924.851523>.

MA, C.; CHEN, M.; KIRA, Z.; ALREGIB, G. TS-LSTM and temporal-inception: Exploiting spatiotemporal dynamics for activity recognition. **CoRR**, abs/1703.10667, 2017. Disponível em: <http://arxiv.org/abs/1703.10667>.

NANNI, L.; GHIDONI, S.; BRAHNAM, S. Handcrafted vs. non-handcrafted features for computer vision classification. **Pattern Recognition**, Elsevier, v. 71, p. 158–172, 2017.

NG, J. Y.-H.; HAUSKNECHT, M.; VIJAYANARASIMHAN, S.; VINYALS, O.; MONGA, R.; TODERICI, G. Beyond Short Snippets: Deep Networks for Video Classification. In: **IEEE Conference on Computer Vision and Pattern Recognition**, 2015. p. 4694–4702.

NGO, C.-W.; PONG, T.-C.; CHIN, R. T. Camera Break Detection by Partitioning of 2D Spatio-Temporal Images in MPEG Domain. In: **IEEE International Conference on Multimedia Computing and Systems**, 1999. v. 1, p. 750–755.

NGO, C.-W.; PONG, T.-C.; CHIN, R. T. Detection of Gradual Transitions through Temporal Slice Analysis. In: **IEEE Computer Society Conference on Computer Vision and Pattern Recognition**, 1999. v. 1, p. 36–41.

OJALA, T.; PIETIKAINEN, M.; HARWOOD, D. Performance evaluation of texture measures with classification based on kullback discrimination of distributions. In: **Proceedings of 12th International Conference on Pattern Recognition**, 1994. v. 1, p. 582–585.

PHAM, N.; PAGH, R. Fast and scalable polynomial kernels via explicit feature maps. In: ACM. **Proceedings of the 19th ACM SIGKDD International Conference on Knowledge Discovery and Data Mining**, 2013. p. 239–247.

PINTO, A. da S.; PEDRINI, H.; SCHWARTZ, W.; ROCHA, A. Video-based face spoofing detection through visual rhythm analysis. In: **2012 25th SIBGRAPI Conference on Graphics, Patterns and Images**, 2012. p. 221–228.

SCHULDT, C.; LAPTEV, I.; CAPUTO, B. Recognizing human actions: A local svm approach. In: **Proceedings of the Pattern Recognition, 17th International Conference on (ICPR'04) Volume 3 - Volume 03**, 2004. (ICPR '04), p. 32–36. ISBN 0-7695-2128-2. Disponível em: <http://dx.doi.org/10.1109/ICPR.2004.747>.

SCOVANNER, P.; ALI, S.; SHAH, M. A 3-dimensional sift descriptor and its application to action recognition. In: ACM. **Proceedings of the 15th ACM international conference on Multimedia**, 2007. p. 357–360.

SENGUPTA, B.; QIAN, Y. Pillar networks++: Distributed non-parametric deep and wide networks. **arXiv preprint arXiv:1708.06250**, 2017.

SEVILLA-LARA, L.; SUN, D.; JAMPANI, V.; BLACK, M. J. Optical flow with semantic segmentation and localized layers. **CoRR**, abs/1603.03911, 2016.

SHI, Y.; TIAN, Y.; WANG, Y.; ZENG, W.; HUANG, T. Learning long-term dependencies for action recognition with a biologically-inspired deep network. In: **Proceedings of the IEEE International Conference on Computer Vision**, 2017. p. 716–725.

SIMONYAN, K.; ZISSERMAN, A. Two-Stream Convolutional Networks for Action Recognition in Videos. In: **Advances in Neural Information Processing Systems**, 2014. p. 568–576.

SIMONYAN, K.; ZISSERMAN, A. Very Deep Convolutional Networks for Large-Scale Image Recognition. **arXiv preprint arXiv:1409.1556**, 2014.

SONG, X.; LAN, C.; ZENG, W.; XING, J.; SUN, X.; YANG, J. Temporal-spatial mapping for action recognition. **IEEE Transactions on Circuits and Systems for Video Technology**, IEEE, 2019.

SOOMRO, K.; ZAMIR, A. R.; SHAH, M. UCF101: A Dataset of 101 Human Actions Classes from Videos in the Wild. **arXiv preprint arXiv:1212.0402**, 2012.

SOUZA, M. R. **Digital Video Stabilization: Algorithms and Evaluation**. Dissertação (Mestrado) — Institute of Computing, University of Campinas, Campinas, Brazil, 2018.

SUN, S.; KUANG, Z.; SHENG, L.; OUYANG, W.; ZHANG, W. Optical flow guided feature: a fast and robust motion representation for video action recognition. In: **Proceedings of the IEEE Conference on Computer Vision and Pattern Recognition**, 2018. p. 1390–1399.

SZEGEDY, C.; LIU, W.; JIA, Y.; SERMANET, P.; REED, S.; ANGUELOV, D.; ERHAN, D.; VANHOUCKE, V.; RABINOVICH, A. Going Deeper With Convolutions. In: **IEEE Conference on Computer Vision and Pattern Recognition**, 2015.

SZEGEDY, C.; VANHOUCKE, V.; IOFFE, S.; SHLENS, J.; WOJNA, Z. Rethinking the Inception Architecture for Computer Vision. In: **IEEE Conference on Computer Vision and Pattern Recognition**, 2016. p. 2818–2826.

TORRES, B. S.; PEDRINI, H. Detection of Complex Video Events through Visual Rhythm. **The Visual Computer**, Springer, p. 1–21, 2016.

TRAN, D.; BOURDEV, L.; FERGUS, R.; TORRESANI, L.; PALURI, M. Learning spatiotemporal features with 3d convolutional networks. In: **Proceedings of the IEEE International Conference on Computer Vision**, 2015. p. 4489–4497.

TRAN, D.; WANG, H.; TORRESANI, L.; RAY, J.; LECUN, Y.; PALURI, M. A closer look at spatiotemporal convolutions for action recognition. In: **Proceedings of the IEEE Conference on Computer Vision and Pattern Recognition**, 2018. p. 6450–6459.

TURAGA, P.; CHELLAPPA, R.; SUBRAHMANIAN, V. S.; UDREA, O. Machine recognition of human activities: A survey. **IEEE Transactions on Circuits and Systems for Video Technology**, Citeseer, v. 18, n. 11, p. 1473, 2008.

VALIO, F. B.; PEDRINI, H.; LEITE, N. J. Fast rotation-invariant video caption detection based on visual rhythm. In: SPRINGER. **Iberoamerican Congress on Pattern Recognition**, 2011. p. 157–164.

WANG, H.; KLÄSER, A.; SCHMID, C.; LIU, C.-L. Dense trajectories and motion boundary descriptors for action recognition. **International Journal of Computer Vision**, Springer, v. 103, n. 1, p. 60–79, 2013.

WANG, H.; SCHMID, C. Action Recognition with Improved Trajectories. In: **IEEE International Conference on Computer Vision**, 2013. p. 3551–3558.

WANG, H.; ULLAH, M. M.; KLASER, A.; LAPTEV, I.; SCHMID, C. Evaluation of local spatio-temporal features for action recognition. In: BMVA PRESS. **BMVC 2009-British Machine Vision Conference**, 2009. p. 124–1.

WANG, H.; YANG, Y.; YANG, E.; DENG, C. Exploring Hybrid Spatio-Temporal Convolutional Networks for Human Action Recognition. **Multimedia Tools and Applications**, Springer, v. 76, n. 13, p. 15065–15081, 2017.

WANG, J.; CHERIAN, A.; PORIKLI, F.; GOULD, S. Video representation learning using discriminative pooling. In: **IEEE Conference on Computer Vision and Pattern Recognition**, 2018. p. 1149–1158.

WANG, L.; QIAO, Y.; TANG, X. Action recognition with trajectory-pooled deep-convolutional descriptors. In: **Proceedings of the IEEE Conference on Computer Vision and Pattern Recognition**, 2015. p. 4305–4314.

WANG, L.; XIONG, Y.; WANG, Z.; QIAO, Y. Towards Good Practices for very Deep Two-Stream Convnets. **arXiv preprint arXiv:1507.02159**, 2015.

WANG, L.; XIONG, Y.; WANG, Z.; QIAO, Y.; LIN, D.; TANG, X.; GOOL, L. V. Temporal Segment Networks: Towards Good Practices for Deep Action Recognition. In: SPRINGER. **European Conference on Computer Vision**, 2016. p. 20–36.

WANG, X.; FARHADI, A.; GUPTA, A. Actions˜ transformations. In: **Proceedings of the IEEE Conference on Computer Vision and Pattern Recognition**, 2016. p. 2658–2667.

WANG, X.; GIRSHICK, R.; GUPTA, A.; HE, K. Non-local neural networks. In: **Proceedings of the IEEE Conference on Computer Vision and Pattern Recognition**, 2018. p. 7794–7803.

WANG, Y.; LONG, M.; WANG, J.; YU, P. S. Spatiotemporal Pyramid Network for Video Action Recognition. In: **IEEE Conference on Computer Vision and Pattern Recognition**, 2017. p. 2097–2106.

WANG, Y.; TRAN, V.; HOAI, M. Eigen evolution pooling for human action recognition. **arXiv preprint arXiv:1708.05465**, 2017.

WEINLAND, D.; RONFARD, R.; BOYER, E. A survey of vision-based methods for action representation, segmentation and recognition. **Computer Vision and Image Understanding**, Elsevier, v. 115, n. 2, p. 224–241, 2011.

WELFORD, B. Note on a method for calculating corrected sums of squares and products. **Technometrics**, Taylor & Francis Group, v. 4, n. 3, p. 419–420, 1962.

WILLEMS, G.; TUYTELAARS, T.; GOOL, L. V. An efficient dense and scale-invariant spatio-temporal interest point detector. In: SPRINGER. **European Conference on Computer Vision**, 2008. p. 650–663.

YEFFET, L.; WOLF, L. Local trinary patterns for human action recognition. In: **2009 IEEE 12th International Conference on Computer Vision**, 2009. p. 492–497.

ZACH, C.; POCK, T.; BISCHOF, H. A duality based approach for realtime tv-l 1 optical flow. In: SPRINGER. **Joint Pattern Recognition Symposium**, 2007. p. 214–223.

ZEILER, M. D.; FERGUS, R. Visualizing and understanding convolutional networks. In: SPRINGER. **European Conference on Computer Vision**, 2014. p. 818–833.

ZHANG, B.; WANG, L.; WANG, Z.; QIAO, Y.; WANG, H. Real-time action recognition with enhanced motion vector cnns. In: **Proceedings of the IEEE Conference on Computer Vision and Pattern Recognition**, 2016. p. 2718–2726.

ZHANG, H.; SMOLIAR, S. W. Developing power tools for video indexing and retrieval. In: INTERNATIONAL SOCIETY FOR OPTICS AND PHOTONICS. **storage and retrieval for image and video databases II**, 1994. v. 2185, p. 140–150.

ZHU, J.; ZHU, Z.; ZOU, W. End-to-end video-level representation learning for action recognition. In: **2018 24th International Conference on Pattern Recognition (ICPR)**, 2018. p. 645–650.

ZHU, W.; HU, J.; SUN, G.; CAO, X.; QIAO, Y. A Key Volume Mining Deep Framework for Action Recognition. In: **IEEE Conference on Computer Vision and Pattern Recognition**, 2016. p. 1991–1999.